Complex & Intelligent Systems (2026) 12:32
https://doi.org/10.1007/s40747-025-02151-w

ORIGINAL ARTICLE

Stochastic optimization framework for capacity planning of hybrid solar PV–small hydropower systems using metaheuristic algorithms

Edward B. Ssekulima[1] · **Amir H. Etemadi**[1]

Received: 12 June 2025 / Accepted: 11 October 2025

Abstract
The integration of variable renewable energy (VRE) into power systems requires optimal capacity planning to ensure cost-effective and reliable operation. While metaheuristic algorithms are widely applied, there is limited rigorous benchmarking comparing the performance of leading single-objective and multi-objective algorithms within a unified stochastic framework for the hybridization of renewable energy technologies. To bridge this gap, this study develops a stochastic optimization framework and conducts a comprehensive evaluation of six metaheuristics: Non-dominated Sorting Genetic Algorithm II (NSGA-II), Multi-Objective Evolutionary Algorithm based on Decomposition (MOEAD) and Generalized Differential Evolution 3 (GDE3) for multi-objective optimization; and Particle Swarm Optimization (PSO), Differential Evolution (DE), and Genetic Algorithm (GA) for single-objective optimization. The multi-objective approaches aimed to maximize total energy output and minimize energy production cost, while the single-objective methods focused on minimizing the levelized cost of electricity (LCOE). A case study for the hybridization of a small hydropower plant with Solar PV was conducted. The results show that NSGA-II delivered the lowest LCOE of 6.54 US ¢ per kWh with a system capacity of 16.33 MW and a capacity factor of 42.74%. DE outperformed other single-objective methods, offering the lowest mean LCOE of 8.96 US ¢ per kWh, a system capacity of 19.37 MW, and a capacity factor of 49.31%. The proposed framework provides a robust tool for system designers and policymakers to bolster sustainable and economically viable deployment of VRE systems which is central to a clean energy transition.

Keywords Modelling · Simulation · Optimization · Hybrid energy systems · Evolutionary algorithms · Levelized cost of electricity (LCOE)

Introduction

There is overwhelming global support for investment in Renewable Energy Sources (RES) as the cornerstone of a clean energy transition. Therefore, it is not surprising that clean energy investments accounted for about 70% of the growth in the energy sector in 2024 [1]. This level of investment presents a significant shift in the global energy landscape as the world moves towards more sustainable energy sources to allay the impacts of global warming and bolster energy security. Over the past decade, the required upfront investment costs for solar and wind power projects have significantly decreased because of technological improvements, allowing these technologies to reach grid parity in some electrical markets [2–5]. This has made solar and wind the leading RES after hydropower.

The key reasons for the increased power generation based on RES include the following: RES generate electricity with minimal greenhouse gas (GHG) emissions and have lower environmental impacts in comparison with conventional fossil fuel- based power plants; thus, their integration into the power system can significantly reduce GHG emissions and contribute to global efforts to combat climate change [6]. For non-oil producing countries, expanding the share of RES within a country's energy mix can improve energy security by reducing reliance on imported oil, thereby mitigating the risks associated with geopolitical tensions and fluctuating global oil prices [4]. Furthermore, RES can potentially contribute to increasing access to affordable modern energy

✉ Edward B. Ssekulima
balekessekulima@gmail.com; ebssekulima@gwu.edu

[1] School of Engineering and Applied Sciences (SEAS), George Washington University, 2121lSt NW, Washington, DC 20052, USA

Published online: 02 December 2025

services for consumers thereby spurring economic growth, even in rural areas because they can be deployed as decentralized generators (DGs).

Despite its many benefits, power generation based on RES presents several challenges. It poses grid integration hurdles whenever its capacity surpasses approximately 10% of the total capacity of the power system and the ensuing technical and economic issues must be addressed [7]. The main issues stem from the intermittent nature of the resources, which makes their power output uncertain and variable thus posing problems regarding grid stability and power quality [8]. Because their power output is highly variable, wind and solar energy are commonly referred to as variable renewable energy (VRE) resources. However, the variations in hydropower output are largely seasonal. Hydropower plants with capacities below 30 MW are classified as small hydropower, mini hydropower or micro-hydropower plants. Hydropower facilities classified as micro-hydropower have a capacity of less than 100 kW, mini-hydropower facilities have a capacity between 100 kW and 1 MW, and small hydropower plants have a capacity between 1 and 30 MW [9]. To enhance the grid integration of these VRE systems, their inherent variations must be considered during system capacity planning and design.

Some interventions for addressing the challenges posed by VRE include technological approaches encompassing system capacity planning, grid infrastructure expansion, and adapting market and regulatory frameworks to incentivize investment in VRE and facilitate their integration into the power grid [10]. Some technological approaches include the use of pumped-storage hydropower or batteries to store part of the power generated during high-generation intervals and release power during low-generation intervals. Energy storage can further support adherence to the required system ramp rate, which measures how fast a generation facility can change its power output and is typically expressed in MW per minute. Different power systems have different grid code requirements for ramping capabilities [11, 12]. Owing to the high cost of storage, strategies involving demand response management initiatives and time-of-use tariffs are usually deployed to align power demand with VRE generation, which enhances the power system's flexibility and reduces the need for grid-scale energy storage interventions [13]. In addition, VRE sources can be combined with other renewable or conventional generation technologies in hybrid systems to increase the overall system reliability and reduce the effective variability of the hybrid power systems [14].

This study addresses the problem of inappropriate sizing of the installed capacity for power plants that rely on variable energy resources due to inadequate quantification of the uncertainty in the plants' power generation output over their design life, at the planning or feasibility study stage. Specifically, this study presents a methodological contribution to the sizing of hybrid RES based power plants, using stochastic optimization to account for the uncertainty in the primary resources while minimizing the levelized cost of energy (LCOE). In addition, this study presents an approach for augmenting efforts to maximize plant factors when complementary resources are deployed, and energy generation output is maximized. This methodology was applied to a hybrid solar photovoltaic–small hydropower (SPV–SHP) system that considers an existing small-hydropower plant (SHPP) on the Wambabya River in Buseruka, Uganda. Our framework sought to determine the optimal number of hydropower turbines, installed discharge capacity, and size of a solar photovoltaic plant while considering the variability of the resources. The goal of stochastic optimization in this study is to minimize the LCOE of the hybridized plant by maximizing the energy generated from the hybridized systems while minimizing the life cycle costs of the power systems. To the best of the authors knowledge, this is the first time that a stochastic based approach is being used to size a hybrid solar photovoltaic–small hydropower in Uganda. The main contributions of this study can be summarized as below:

- A stochastic capacity planning framework is proposed for hybrid solar PV–small hydropower systems, addressing renewable resource variability using ensemble-based optimization.
- Six metaheuristic algorithms; namely, NSGA-II, MOEAD, GDE3, PSO, DE, and GA are comparatively evaluated under both multi- and single-objective formulations.
- A knee point detection method is employed to extract the most optimal and practically relevant solutions from the Pareto front, supporting effective trade-off analysis in multi-objective optimization.

The remainder of this paper is organized as follows. "Literature review" presents a literature review of the latest approaches to managing variability and sizing hybrid VRE power systems to account for uncertainty. Our methodology is detailed in "Methodology" and is then applied to the case study presented in "Case study description and simulation data". "Results and discussions" presents the study results and discussions, while the key limitations of the study, conclusions, and future work are discussed under "Conclusion and future work".

Literature review

The ever-increasing global call for more renewable energy-based power generation requires that effort be taken to address the inherent variability of the resources right from

the power generation planning stage, which is key for their grid integration. This can be partly achieved by critically considering the generation facilities as systems within a larger power system. Therefore, a System of Systems (SoS) perspective is paramount for the effective grid integration of VERS and optimal operation of the power system. The key stakeholder requirements relate to the system's LCOE (which informs the tariff regime), environmental considerations, system reliability, and ancillary services such as voltage and frequency control [15]. Several approaches to address these requirements have been documented in the literature. These include VRE resource forecasting, reserve management, grid flexibility measures, hybridization, and the appropriate sizing of power plants.

Variable renewable energy sources

The term variable renewable energy (VRE) is mainly used to refer to solar photo-voltaic (PV) and wind energy-based generation plants, as these resources exhibit the greatest variability across the entire range of the temporal horizon (seconds, minutes, hours, and days). The variability in other renewable energy sources, such as hydropower and biomass, is seasonal in nature and therefore spans several days or months.

VRE generation forecasting techniques

Accurate forecasting of renewable energy generation and load demand is critical and cost-effective for the optimal capacity planning and operation of VRE systems and their grid integration. The intent is to estimate the power output of the generation plants as precisely as possible for the short term (minutes, hourly, and daily) to facilitate various operations of the power system [16, 17]. Figure 1 depicts various applications of forecasts in the operation of a power system (considering interconnection, transmission, and distribution segments). Several scholars have investigated and documented various forecasting techniques, such as time-series analysis and machine-learning-based methods, including hybridized techniques, to provide accurate forecasts of VRE generation at various timescales [18–20]. It is imperative to note that these forecasts primarily rely on the historical weather data of the respective geographical locations as the key input to the models.

Reserve management and grid flexibility measures

Adequate reserves are required to manage the fluctuations and ramp events associated with VRE generation in grid integrated systems. Several studies have explored optimal reserve management strategies, considering both conventional and demand-side flexibility options. Power system/grid operators typically conduct grid flexibility studies to determine the amount of VRE that can be integrated into the grid while maintaining the desired reliability and system flexibility levels. The grid flexibility measures employed include maintaining appropriate standing and spinning reserves (particularly in more flexible power plants), demand response approaches, and energy storage [12, 21–23].

Sizing hybrid VRE systems

With the on-going global transition towards higher penetration levels of renewable energy, the role of hybrid VRE systems has become more critical. Some of the challenges associated with the intermittency of VRE can be addressed through resource hybridization. This involves combining different technologies, such as solar photovoltaics, wind, and hydropower. The sizing of hybrid VRE aims to strike a compromise between system cost, reliability, and environmental impact [24]. Numerous approaches have been used to address these challenges, ranging from traditional optimization techniques to sophisticated machine learning (ML) and artificial intelligence (AI) methodologies which have undergone significant advancement over the past decade.

Several optimization methods, including Genetic Algorithms (GAs), Particle Swarm Optimization (PSO), Ant Colony Optimization (ACO), and non-dominated sorting genetic algorithm II (NSGA-II), have been used to solve the hybrid sizing problem [25, 26]. The algorithms search within the solution space to determine the ideal system size that maximizes the performance and reliability while minimizing expenses. However, these techniques require intricate mathematical formulations and significant computational resources. Machine-learning techniques are now commonly used in hybrid VRE sizing because of the algorithm's ability to learn from historical data and manage complex relationships [27]. To simplify the sizing procedure, deep-learning techniques can be applied to simulate the linkages between different system parameters and the capacity of the system. However, if not appropriately modelled, these algorithms can suffer from overfitting and require a large amount of data.

To effectively manage the integration of VRE, new grid technologies, including smart grids and microgrids, have attracted interest from both the research community and industry. These solutions provide enhanced control and flexibility, thereby offering enhanced management of the intermittency inherent in VRE. Therefore, it is not surprising that the use of sophisticated modeling and simulation tools to aid the planning, design, and day-to-day operation of VRE-based power stations has become prominent in recent studies [15]. These technologies combine intricate models of the load, ESS, and renewable energy sources, enabling more

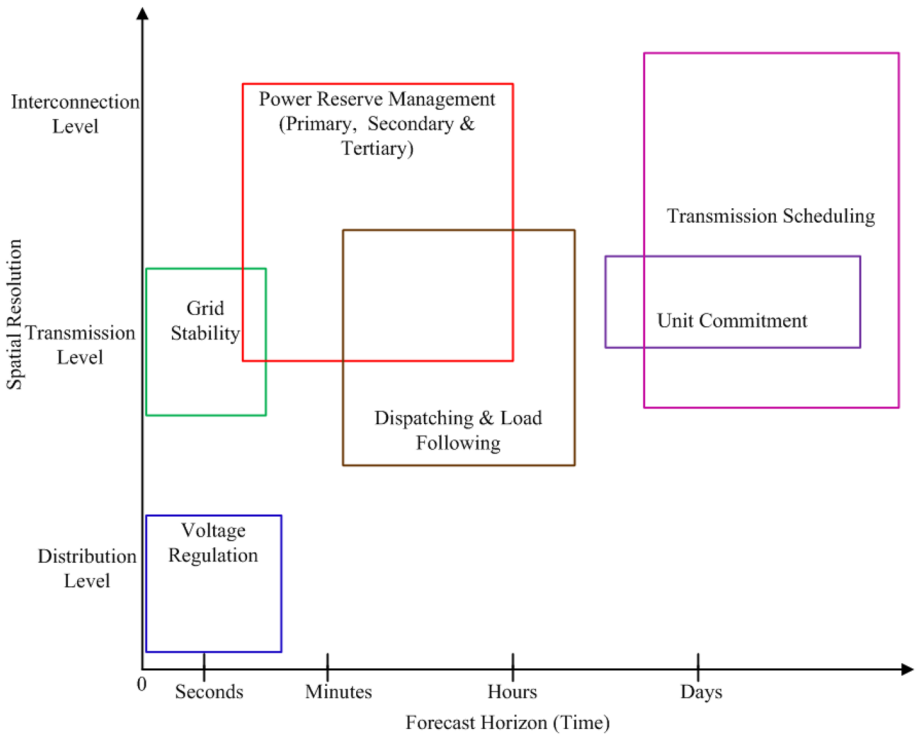

Fig. 1 Applications for forecasts in power system operations (source: Authors)

precise sizing and better system performance. The combination of complementary technologies, such as wind and solar PV, has also been shown to result in better grid integration of hybrid VRE systems and enhancement of the plant capacity factor which is the ratio of the energy generated by a generating plant in each period to the energy it would have generated over the same period, at its full installed capacity.

Several opportunities still exist for enhancing the grid integration of VRE. However, there are limited studies on the hybridization of small hydropower plants with solar PV, yet the two technologies are complementary in nature considering seasonality aspects and could therefore benefit power system operators if optimally sized with a clearly defined power generation management regime for the hybrid power plant. Further studies are necessary to develop reliable and comprehensive solutions aimed at bolstering the grid integration of VRE.

Gaps in the recent state of the art developments

Multi-objective optimization techniques have been employed to balance multiple objectives, such as system reliability, cost, and environmental performance, when sizing hybrid renewable energy systems [28]. To account for fluctuations and uncertainty in the VRE output, optimization approaches relying on ML techniques and stochastic approaches have been employed to size hybrid systems in several studies. However, despite advances in stochastic approaches, several gaps remain unaddressed. The major gaps are related to uncertainty quantification, in which the uncertainties associated with renewable energy resource availability, load demand, and system component performance may not be fully captured by existing stochastic approaches. The aspect of computational complexity also manifests when optimizing large-scale hybrid systems.

In this study, we propose the use of evolutionary algorithms combined with stochastic optimization techniques to address the system capacity sizing challenge for a hybrid small-hydro solar photovoltaic power plant. This can provide valuable insights to developers and system operators when undertaking VRE system capacity planning, grid-integration and flexibility studies.

Methodology

Power generation in VRE sources follows the variation in the primary fuel resource (solar irradiance, water flows, wind speed, etc.) as opposed to fossil-based production, where the power output can be pre-determined and easily regulated. The fluctuation in the resource can be modelled using stochastic nomenclature, considering a simulation environment linking power generation, $\underline{p_g}$, with the meteorological input process denoted as $\underline{x}$, where the underline notation has been used to denote a stochastic process throughout this paper.

Table 1 below provides a list of the core symbols used in this paper.

Table 1 List of symbols

Symbol	Meaning and units
ρ	Density of water (kg/m^3)
g	Gravitational acceleration (9.81 ms^{-2})
K	Rated power output capacity (kW)
$p_{g_o}(\underline{x})$	Theoretical power output (kW)
$\eta(\underline{x})$	System efficiency (%)
$\underline{H}$	Gross hydraulic head for a hydropower plant (m)
H_{net}	Net hydraulic head (m)
Q_{design}	Design discharge (m^3/s)
Q_{Tr}	Rated discharge per turbine (m^3/s)
$\underline{Q}_T$	Hourly average turbined discharge (m^3/s)
η_{Tr}	Nominal turbine efficiency (estimated at 90% [29])
$\eta_T(t)$	Turbine efficiency (%) at time, t
n_{hyd}	Number of turbines
$\{a, b, c\}$	Hydro turbine efficiency factors as detailed in [30]
η_G	Generator efficiency (estimated at 90% [29])
$E_{hyd}(t)$	Hourly average energy output of the SHPP (kWh)
C_{hyd_i}	Initial investment costs for hydropower (US$)
C_{hyd_mtc}	Maintenance cost for hydropower (US$)
C_h	Cost per kW of hydropower capacity (US$)
G_{pv}	Solar irradiance (kWh m^{-2})
A_{pv}	Area of one PV module's surface (m^2)
n_{pv}	Number of PV modules
E_{pv}	Energy generated by Solar PV (kWh)
η_{pv}	Conversion efficiency of the PV modules (%)
C_{pv_i}	Investment costs for solar PV (US$)
C_{pv_mtc}	Maintenance costs for solar PV (US$)
t	Time (h)
T	Total number of hours over the design period of 25 years i.e., $T = 219{,}000$
C_{Total}	Total levelized cost of the generated energy of the hybridized system
E_{Total}	Total levelized energy output of the hybridized system

Problem formulation

We consider the capacity planning for a grid-connected hybrid plant comprising a run-of-river small hydropower plant (SHPP) and utility-scale solar photovoltaic (PV). The overall goal is to minimize the levelized cost of energy (LCOE) which is achieved by simultaneously minimizing the total levelized cost of the generated energy, C_{Total}, while maximizing the total levelized energy output E_{Total} of the hybrid system. The problem can therefore be construed as either a bi-objective function or single objective function.

Bi-objective problem formulation

Objective 1:

$$\min. f_1(x) = C_{Total} \tag{1}$$

Objective 2:

$$\max. f_2(x) = E_{Total} = \sum_{t=1}^{T} E \tag{2}$$

where:

- $C_{Total} = [(C_{hyd\_i}(x) + C_{pv\_i}(x)) + \sum_{t=1}^{T}\left[C_{hyd\_mtc} + C_{pv\_mtc}\right]/(1+r)^{k(t)}]$
- $C_{hyd\_i}(x) = C_h.\rho.g.H_{net}.\eta_G.\eta_{Tr}.Q_{Tr}.n_{hyd}$
- $E = \left[E_{hyd}(x) + E_{pv}(x)\right]/(1+r)^{k(t)}$
- $k(t) = \lceil t/h_y \rceil$ where $h_y = 8760$ $(hours\ in\ a\ year)$
- $x \in \{n_{pv},\ Q_{Tr},\ n_{hyd}\}$
- $E_{hyd}(x) = \rho.g.\underline{Q}_T(t).H_{net}.\eta_G.\eta_T(t)$
- $E_{pv}(x) = \eta_{pv}(t).G_{pv}(t).A_{pv}.n_{pv}$
- r is the discount rate (economic opportunity cost of capital) which is taken as 11% based on the Uganda National Parameters [31].

Single objective problem formulation

The single objective formulation minimizes the LCOE generated from the hybrid power system over its design-life of $T = 25$ years, as a single function. This approach is represented by Eq. (3).

$$\min.\{f_1(x)/f_2(x)\} \tag{3}$$

The generation resource constraints and bounds are same for both the bi-objective and single objective formulations.

Numerical bounds and affordability (LCOE) constraint

1) PV module count (n_{pv}) : The Solar PV plant is sized between 5 and 10 MWp to guarantee a minimum PV share of 30% of the hybrid plant's nameplate when the SHPP's capacity $\leq$ 10 MW, and to avoid a PV nameplate exceeding the maximum SHPP generation potential (10.2 MW in 2022). Therefore, using the selected Maxeon SPR-MAX6-440, 440 W module, whose data sheet is provided in [32], the bounds are:

$n_{pv}^{min} = 5{,}000{,}000/440 = 11{,}364$ and $n_{pv}^{max} = 10{,}000{,}000/440 = 22{,}728$;

Hence, $11{,}364 \leq n_{pv} \leq 22{,}728$. The 5 MWp lower limit is the smallest PV size that robustly satisfies a $\geq$ 30% PV

share once DC/AC derates and operating conditions are considered; the 10 MWp upper limit keeps the PV capacity at or below the SHPP's recorded maximum (10.2 MW).

2) Number of hydro turbines/units (n_{hyd}): We restrict the number of turbines to 2–4 units so that the plant can track demand and seasonal flow variations with adequate part-load efficiency and outage resilience as recommended in hydropower design practice [33]; thus $2 \leq n_{hyd} \leq 4$.

3) Nominal/rated per turbine discharge (Q_{Tr}): With the site design discharge derived from the FDC (see "Simulation data") being $Q_{design} = 3.518 m^3/s$, the per unit nominal turbine discharge is:

$$Q_{Tr} = \frac{Q_{design}}{n_{hyd}} = \begin{cases} n_{hyd} = 4 : Q_{Tr} = 0.88\ \mathrm{m}^3/s, \\ n_{hyd} = 3 : Q_{Tr} = 1.17\ \mathrm{m}^3/s\ , \\ n_{hyd} = 2 : Q_{Tr} = 1.76\ \mathrm{m}^3/s. \end{cases}$$

Therefore, the feasible range across unit counts is $0.88 \leq Q_{Tr} \leq 1.76\ \mathrm{m}^3/\mathrm{s}$.

4) Affordability (LCOE) constraint: We impose $[C_{Total}/E_{Total}] \leq 0.11$ US$/kWh to exclude cost-dominated designs and keep results within acceptable feed-in-tariffs informed by the fact that the highest tariff for existing renewable energy based plants in Uganda is US ¢ 11 per kWh.

A summary of the bounds and constraint used in the optimization model is given below.

$$11364 \leq n_{pv} \leq 22728$$

$$2 \leq n_{hyd} \leq 4$$

$$0.88 \leq Q_{Tr} \leq 1.76\,\mathrm{m}^3/\mathrm{s}$$

$$[C_{Total}/E_{Total}] \leq 0.11\ \mathrm{US\$/kWh}$$

Energy and cost models for variable renewable energy sources

The input process, $\underline{x}$, is transformed through a non-linear function into a power output variable, $\underline{p_g}$, through (4).

$$\underline{p_g}(\underline{x}) = \begin{cases} 0 & \underline{x} < \underline{x}_{min} \\ \eta[\underline{x}] p_{g_o}[\underline{x}] & \underline{x}_{min} \leq \underline{x} < \underline{x}_{max} \\ K & \underline{x}_{max} \leq \underline{x} < \underline{x}_s \\ 0 & \underline{x} \geq \underline{x}_s \end{cases} \quad (4)$$

Both the theoretical and nominal power are driven by $\underline{x}$. The limits $\underline{x}_{min}$ and $\underline{x}_{max}$ are associated with a specific VRE resource, where $\underline{x}_{min}$ represents the minimum value of the primary energy resource necessary to commence power generation and $\underline{x}_{max}$ is the value of the primary energy resource at rated power. $\underline{x}_s$ denotes the maximum primary resource input, which is a constraint, beyond which power generation is stopped to maintain the system integrity. "The theoretical power output depends on the location, design layout and associated technical parameters for the specific VRE resource under consideration" [34].

Hydropower

The theoretical power generated by a hydropower plant is largely dependent on the available head and river discharge /flow as shown in (5).

$$p_{g_o}\left(\underline{H}, \underline{Q}_T\right) = \rho g \underline{Q}_T \underline{H} \quad (5)$$

The limits $\underline{Q}_{T\,min}$, $\underline{Q}_{T\,max}$ and $\underline{Q}_{T\,s}$ are determined by specific turbine characterization. It is imperative to note that the turbine flow is a spatiotemporal control of the runoff generated over the plant's catchment area and harnessed through a hydraulic system encompassing diverting (and in some cases storage) of the flow and conveyance through a penstock (for small hydros). The primary stochastic process representing the stream flow is subjected to constraints such as environmental flow, reservoir and penstock capacities as well as the limitations imposed by the turbine characteristics. Changes in $\underline{H}$ emanate from fluctuations in the intake level, upstream since the tailrace remains at the same elevation. The overall system efficiency, $\eta(\underline{x})$ was determined by multiplying the respective efficiencies of the different components. For hydropower plants, this encompasses losses due to hydraulics in the penstock and the mechanical, mass and hydraulic losses due to the turbine, generator and transformer power losses. It is challenging to construct precise mathematical representations of these efficiencies because they are typically governed by intricate physical principles [30]. Typically, nomographs, supplied by the manufacturer based on the test results, represent the efficiency function unique to each equipment type. It may suffice to note that many studies provide for the electrical generator efficiency to be at least 90% [35], and the same was used in this study.

Turbine efficiency model A turbine type is selected based on the estimated turbine flow and net head of the plant. A turbine selection nomograph for small and mini-hydro power plants, as presented in [36] is shown in Fig. 2 and was the basis for selecting the turbine type in this study. In principle, nomographs aid the selection of the appropriate turbine type based on the river flows and available head. Equation (6) is used to determine the turbine efficiency, and is based on the

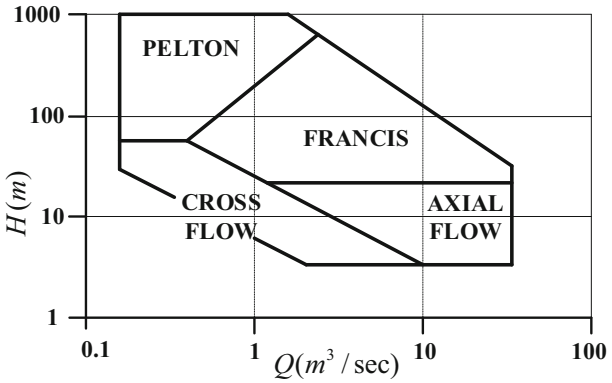

Fig. 2 Turbine selection nomograph

experimental data presented in [30].

$$\eta_T(t) = \left[a\left(\frac{Q_T(t)}{n_{hyd} \cdot Q_{Tr}}\right)^2 + b\left(\frac{Q_T(t)}{n_{hyd} \cdot Q_{Tr}}\right) + c\right].\eta_{Tr} \tag{6}$$

Cost model for the small hydropower plant The power generation cost for a small hydropower plant denoted as $C_{hyd}[\text{US\$}]$ is a summation of the costs for the investment (initial capital outlay), $C_{hyd\_i}[\text{US\$}]$ and those for maintenance, $C_{hyd\_mtc}[\text{US\$}]$, of the plant.

C_{hyd} depends on the net available head, rated power output and total number of turbines, n_{hyd} which is one of the decision variables in this study. The cost per kW (C_h) is estimated at US$ 3,563 within the 95th percentile of the weighted average cost of hydropower plants with capacities below 50 MW for 2021 [32]. C_{hyd_mtc} was taken to be approximately 5% of the initial capital outlay/investment costs which is aligned with the analysis presented in [37] for small hydropower projects whose operation and maintenance is generally higher than for large hydropower plants.

Solar photovoltaic

For photovoltaic (PV) solar systems, theoretical power is given by (7).

$$p_{g_o}(G_{pv}) = G_{pv} \cdot A_{pv} \cdot n_{pv} \tag{7}$$

The Solar PV module's nominal (nameplate) power is defined at a plane of array irradiance of $G_{pv} = 1000\,\text{W/m}^2$ under Standard Test Conditions (STC: Air Mass of 1.5 spectrum and cell temperature of 25 °C). Equation (8) represents the energy generated by the Solar PV modules. The PV module used in this study was the SunPower Maxeon SPR-MAX6-440 [32].

$$E_{pv}(t) = \eta_{pv}(t) \cdot G_{pv}(t) \cdot A_{pv} \cdot n_{pv} \tag{8}$$

The efficiency, η_{pv} of each module as depicted determined using Eq. (9) as a product of several efficiencies namely; dust, η_d, adaptability of the modules η_{ad}, heating within the cables, η_{cb}, temperature η_{temp} and inclination of the modules η_{in}.

$$\eta_{pv}(t) = \eta_d(t) \cdot \eta_{ad}(t) \cdot \eta_{in}(t) \cdot \eta_{cb}(t).\eta_{temp}(t) \tag{9}$$

The estimated values for the efficiencies η_d, η_{ad}, η_{in} and η_{cb} were 98, 96, 97.3 and 97.8%, respectively as adapted from previous works [38–40]. The η_{temp} term is dependent on additional parameters as shown in Eq. (10).

$$\eta_{temp}(t) = \eta_{pv_{STC}} \cdot [1 + \alpha_t(T_{a\_t} - T_{a\_STC})] \tag{10}$$

where $\eta_{pv_{STC}}$ is the PV module's energy conversion efficiency, based on standard test conditions (STC). α_t is the temperature coefficient of the maximum module power output which for the Maxeon SPR- MAX6-440 is $-0.0029\ ^\circ\text{C}^{-1}$[32].

Solar PV cost model The power generation costs for the solar PV, $C_{pv}[\text{US\$}]$ as presented in Eq. (11) is calculated as the summation of the costs for initial investment $C_{pv\_i}[\text{US\$}]$, maintenance,$C_{pv\_mtc}[\text{US\$}]$ and that for the inverters $C_{pv\_inv}[\text{US\$}]$.

$$C_{pv} = C_{pv\_i} + C_{pv\_mtc} \tag{11}$$

C_{pv_i} is calculated using Eq. (12), where P_{pv_i} is the rated capacity of the solar PV plant in kWp as given by Eq. (13) and $C_{pv/\text{kWp}}$ is the cost per kWp which was estimated to be US$1,276.5, which is the average of the 5th and 95th percentile values of the total installed costs for PV projects in 2023 as published by the International Renewable Energy Agency [41].

$$C_{pv\_i} = P_{pv\_i} \times \left[C_{\frac{pv}{\text{kWp}}} + C_{pv_{inv}/\text{kWp}}\right] \tag{12}$$

$$P_{pv\_i}[\text{kWp}] = n_{pv} \times P_{pv\_r} \tag{13}$$

n_{pv} is one of the decision variables in this study and P_{pv_r} is the rated capacity of one PV module which for the Maxeon SPR-MAX6-440 is 0.44 kWp. C_{pv_mtc} was estimated to be US$14.1/kWp [41]. The inverter cost per kilo-watt peak, denoted as $C_{pv_{inv}/\text{kWp}} = \text{US\$71/kWp}$ [42].

Solution approach

In this study, six well-established evolutionary algorithms are employed: the NSGA-II, MOEAD, and GDE3 for solving the bi-objective optimization problem, and the GA, DE and PSO algorithm for the single-objective case. The choice of these algorithms is guided by a detailed evaluation of their respective strengths and limitations.

Stochastic optimization framework

To account for the inherently intermittent nature of solar and hydropower resources, the optimization framework incorporates stochastic modeling. This ensures that the derived optimal parameters closely mirror the actual behavior and constraints of the hybrid PV-small hydro power plant over its life cycle. The entire optimization framework is implemented in Python [43], leveraging its robust scientific computing ecosystem. The goal is to identify the most suitable system configuration—defined by key decision variables (n_{pv}, Q_{Tr} and n_{hyd}) and an affordability constraint on tariff/LCOE.

Algorithm 1 presents the optimization framework used in this study. The first stage of data processing involves ascertaining that the daily river flow considered for power generation off-sets the environmental flow which for Wambabya river is 0.22 cubic meters per second. A characterization of the uncertainties in the primary energy resources, namely, solar irradiance and river discharge variability was undertaken to ensure that the seasonal and annual variations in the resources are incorporated. This was achieved partly through the identification of the distribution that provided the best fit of the river discharge data and by using Monte Carlo simulation, bootstrapping techniques and the optimization algorithms.

Additionally, the process ensures that the solar irradiation data used takes into consideration the nominal irradiance of 1000 W/m^2. The Monte Carlo simulation is set up by first undertaking stochastic processing of the hydrology data to generate $n \times T$ years of synthetic river flow (the generated daily average river flow was held constant over the respective 24-h period), where n was 100 ensembles and T is the project design life of 25 years. Each ensemble comprised $365 \times 24 \times 25$ values for the average daily hourly river flow and hourly global solar irradiance. Daily hourly temperature and daily hourly global irradiance ensembles were generated using the bootstrapping technique which employs sampling with replacement. The raw 25 years' data were arranged in accordance with the hour of the year (from hour 1 to 8760) resulting in 25 sets from which sampling for each hour of the year was performed with replacement for each of the 100 ensembles. Bootstrapping was applied concurrently to both irradiance and temperature data since both inputs must be applied together. This enabled the generation of n equally probable states and the formulation of n Monte Carlo simulation scenarios by arranging the resource drivers (river flows, solar irradiance and temperature) into n ensembles of T year-length and then sampling random input states into the optimization procedures.

Algorithm 1 Hybrid system capacity planning

Input: Hourly hydrology D_h, irradiance D_s, temperature D_t; technical/economic parameters; bounds; settings {mode $\in$ {SINGLE, MULTI}, S, P, G, }
Output: *CombinedReport* = (single-objective optimum) $\cup$ (multi-objective Pareto & knee)
$D \leftarrow$ PREPROCESSANDRESAMPLETOHOURLY(D_h, D_s, D_t)
$\mathcal{E} \leftarrow$ BUILDSYNTHETICENSEMBLES(D, S)
Define decision vector $x = [n_{\text{hyd}}, Q_{\text{TR}}, n_{\text{pv}}]$; constraints $g(x) \leq 0$, $h(x) = 0$
if mode = SINGLE **then**
    Print: "Proceed to Algorithm 2 (PSO/GA/DE)"
    SingleObj $\leftarrow$ RUN_ALGORITHM_2$(\mathcal{E}, \text{Bounds}, \text{Settings})$
else
    Print: "Proceed to Algorithm 3 (NSGA-II/MOEA/D/GDE3)"
    MultiObj $\leftarrow$ RUN_ALGORITHM_3$(\mathcal{E}, \text{Bounds}, \text{Settings})$
end if
CombinedReport $\leftarrow$ PACKAGERESULTS(*SingleObj*, *MultiObj*)
return *SingleObj*, *MultiObj*, *CombinedReport*

The next step is to select the objective function whether it is single or multi-objective to enable the setting of the optimization problem by selecting the appropriate algorithm. The optimization procedures for single objective and multi-objective formulations are presented in Algorithm 2 and Algorithm 3 respectively.

Algorithm 2 Single-objective optimization—PSO/GA/DE

Input: Ensembles $\mathcal{E}$, bounds, settings; chosen engine $E \in \{\text{PSO}, \text{GA}, \text{DE}\}$
Output: x^* minimizing $\text{LCOE}(x)$ across ensembles; report $\text{ENERGY}(x^*)$, $\text{CF}(x^*)$
$J(x) \leftarrow \text{LCOE}(x)$; set P, G; choose constraint handling (penalty/repair)
Engine params: PSO (ω, c_1, c_2); GA (selection, SBX, PM, elitism); DE (strategy, F, CR)
for $s = 1$ **to** S **do**
  $\mathcal{P} \leftarrow \text{INITIALIZEPOPULATION}(P, \text{Bounds}, \text{seed}_s)$
  Evaluate J on ensemble s; apply constraints
  for $t = 1$ **to** G **do**
    if $E = \text{PSO}$ **then**
      $\text{UPDATEVELOCITIESANDPOSITIONS}(\mathcal{P}; \omega, c_1, c_2)$; $\text{PROJECTTOBOUNDS}()$
    else if $E = \text{GA}$ **then**
      $\mathcal{M} \leftarrow \text{SELECT}(\mathcal{P})$; $\mathcal{O} \leftarrow \text{CROSSOVER+MUTATE}(\mathcal{M})$
      $\mathcal{P} \leftarrow \text{ENVIRONMENTALSELECTION}(\mathcal{P} \cup \mathcal{O}, P)$
    else ▷ $E = \text{DE}$
      $\mathcal{T} \leftarrow \text{MUTATEANDCROSSOVER\_DE}(\mathcal{P}; F, CR, \text{strategy})$
      $\mathcal{P} \leftarrow \text{GREEDYSELECTION\_DE}(\mathcal{P}, \mathcal{T}, J)$
    end if
    Evaluate J; apply constraints; update best x_s^*
  end for
end for
$x^* \leftarrow \text{AGGREGATEACROSSENSEMBLES}(\{x_s^*\})$
return x^*, $\text{LCOE}(x^*)$, $\text{ENERGY}(x^*)$, $\text{CF}(x^*)$

A systematic and iterative computational approach is employed to search for the optimal design configuration. For each simulation scenario, the optimization algorithm selects a set of design parameters, which are within the predefined bounds and constraints, and evaluates their performance using the energy and cost models. These models compute the corresponding objective function, which are then used as feedback to guide the algorithm's search direction in the decision space. This feedback loop enables the algorithm to refine the selection of parameters through evolutionary operations such as selection, crossover, and mutation. The goal is to progressively identify parameter combinations that optimally satisfy the conflicting objectives of maximizing energy output and minimizing cost. Each new candidate solution is evaluated through simulation, and the results inform the next generation of solutions. This iterative process continues until a convergence criterion is met—either when the change in objective function values becomes negligibly small or when a predefined maximum number of function evaluations is reached. Upon completion of the optimization process, the algorithm records the set of parameters that yield the best objective function values for each scenario. These optimal configurations are then analyzed to determine the most suitable system design.

Parameter settings for the algorithms

To support reproducibility of results, the parameter settings for the single-objective and multi-objective algorithms are shown in Tables 2 and 3 respectively. A random seed of 1 was used across all algorithms.

Table 2 Parameter settings for the single-objective algorithms

Algorithm	Parameter description	Parameter settings and rationale
GA	Population, N	We set $N = 100$ to maintain adequate genetic diversity while balancing evaluation budget. *The same is set for PSO and DE.* This is a practical approach that supports performance comparison as espoused in [44]
	Selection and survival	Based on [45, 46], we employed tournament selection elitism, with tournament size $k = 2$ *(i.e., keep best 2).* This applied mild pressure while preserving the top two solutions
	Crossover and mutation	The simulated binary crossover (SBX) with polynomial mutation are used [47, 48]. The crossover probability, $p_c = 1.0$, and mutation probability is $p_m = 1/n$ where n is the number of decision variables. The distribution indexes for crossover and mutation are, $\eta_c = 20$ and $\eta_m = 20$, respectively
	Stopping criterion	This was based on number of function evaluations ($nEvals$), and we set it to $nEvals = 1500$. This provides pragmatic convergence as evidenced in the convergence plot form the trial runs
PSO	Population size (N)	$N = 100$
	Inertia weight (w) and learning factors c_1 and c_2	As recommended in [49, 50], a linearly decreasing strategy was adopted, $w : 0.9 \rightarrow 0.4$; and $c_1 = c_2 = 2$
	Stopping criterion	$nEvals = 1500$
DE	Population size (N)	$N = 100$
	Sampling	The Latin hypercube sampling (LHS) was adopted due to its ability to maximize coverage of the parameter space and enhance the efficiency of the optimization process [51]
	Mutation strategy	We adopt the DE/rand/1/bin strategy which is the default in pymoode and is recommended in [52]
	Cross-over rate (CR) and scale factor (F)	Based on [52], we selected a moderate $CR = 0.5$ and randomized $F = (0.0, 0.9)$ to improve robustness
	Dither and jitter	We set dither to *vector* since selecting F randomly for each difference vector can improve convergence; jitter is set to *False* to ensure no perturbation is added to the difference vectors [53, 54]
	Stopping criterion	$nEvals = 1500$

Table 3 Parameter settings for the multi-objective algorithms

Algorithm	Parameter(s)	Parameter settings and rationale
NSGA-II	Population size, N	***N= 100.*** This ensured that the Pareto-front resolution is balanced with the high cost of hourly/multi-year stochastic simulations and gives approximately a 1% spacing along the normalized front which is sufficient to clearly show the tradeoffs while keeping the runtime reasonable. This choice is consistent with the approach followed in [55, 56]
	Crossover and mutation	Based on [57], the simulated binary crossover (SBX) with polynomial mutation was used. The crossover probability, $p_c = 1.0$, and mutation probability is $p_m = 1/n$ where n is the number of decision variables (for the problem at hand, $n = 3$). The distribution indexes for crossover and mutation are, $\eta_c = 20$ and $\eta_m = 20$, respectively
	Stopping criterion	This was based on maximum number of generations ($mGen$): $mGen = 200$ and the solution ranges usually stabilize by 200 generations as supported by literature [58]. *The same was used for NSGA-II and GD-3 for fair comparison*

Table 3 (continued)

Algorithm	Parameter(s)	Parameter settings and rationale
MOEAD	Reference directions, number of partitions (H) and population size, N	We set reference directions via the Das-Dennis configuration to obtain an even reproducible spread of sub-problems along the bi-objective pareto curve. Under this scheme, the number of reference directions is $N = \binom{H+k-1}{k-1}$; for two objectives, $k = 2$ and $N = H + 1$. Accordingly, we set $H = 100$, yielding $N = 101$ directions (and population). This choice follows the standard decomposition-based EMO practice and the combinatorial characterization of Das–Dennis reference sets reported in literature [59, 60]
	Decomposition type	Penalty Boundary Intersection (PBI) was used as it has been shown to effectively balance convergence and diversity by combining the projection distance along a reference direction with a penalized perpendicular distance, thereby ensuring a uniform Pareto front coverage [61]. A penalty parameter, theta, $\theta = 5$ was adopted as it offers a robust trade-off between spread and convergence [61]. In addition, the tariff cap constraint was handled through the integration of an external penalty into the objectives, and the violation was scaled by a factor beta, which was tuned to $\beta = 80$. This ensures expedited feasibility recovery without over penalization
	Crossover and mutation	Same as NSGA-II (i.e., SBX with polynomial mutation)
	Neighborhood size, T; the probability used to select parents locally, δ and the maximum number of candidate solutions replaced by each offspring solution, n_r	As used in [62, 63], we set: $T = 20;\ \delta = 0.9$ *and* $n_r = 2$
	Stopping criterion	$mGen = 200$
GDE3	Population size, N	We used $N = 100$ to provide robust diversity and for comparability with NSGA-II and MOEAD
	Mutation Strategy	We adopt the DE/rand/1/bin strategy which is the default in pymoode and is recommended in [52]. The strategy avoids early convergence while balancing exploration and exploitation thereby providing a good mechanism for generating diverse candidate solutions and improving them in subsequent generations
	Crossover rate (CR) and Scale Factor (F)	We explored different values of CR and F, taking into consideration the non-linearity structure of the problem which is non-separable and mixed integer. Based on guidance in [52], we selected a moderate $CR = 0.5$ and randomized $F = (0.0, 0.9)$ to improve robustness
	Selection/survival	Pareto dominance and crowding distance [52]
	Stopping criterion	$mGen = 200$

selection of the knee point. The knee point represents a

Algorithm 3 Multi-objective optimization—NSGA-II/MOEA/D/GDE3

Input: Ensembles $\mathcal{E}$, bounds, settings; chosen engine $M \in \{\text{NSGA-II}, \text{MOEA/D}, \text{GDE3}\}$
Output: Aggregated Pareto set $\mathcal{P}^\star$; knee solution x° with metrics
$F_1(x) \leftarrow -\textsc{Energy}(x)$; $F_2(x) \leftarrow \text{LCOE}(x)$
Set P, G; pick ops (SBX+PM or DE); choose constraint handling
Engine specifics: NSGA-II (fast sort, crowding, elitism); MOEA/D (weights, Tchebycheff/PBI, neighborhood T); GDE3 (DE variation, nondom. sort, crowding truncation)
for $s = 1$ **to** S **do**
  $\mathcal{P} \leftarrow \textsc{InitializePopulation}(P, \text{Bounds}, \text{seed}_s)$
  Evaluate $F(x)$; handle constraints
  for $t = 1$ **to** G **do**
    if $M = \text{NSGA-II}$ **then**
      $\mathcal{O} \leftarrow \textsc{Variation\_SBX\_PM}(\mathcal{P})$; $\mathcal{U} \leftarrow \mathcal{P} \cup \mathcal{O}$
      Fronts $\leftarrow \textsc{FastNonDominatedSort}(\mathcal{U})$; CD $\leftarrow \textsc{CrowdingDistance}$(Fronts)
      $\mathcal{P} \leftarrow \textsc{SelectByRankThenCrowding}(\text{Fronts}, \text{CD}, P)$
    else if $M = \text{MOEA/D}$ **then**
      for each subproblem i with weight w_i **do**
        Parents $\leftarrow \textsc{Neighbors}(\mathcal{P}, i, T)$; $y \leftarrow \textsc{Variation}$(Parents)
        for $j \in \textsc{Neighbors}(i)$ **do**
          if $\textsc{Agg}(F(y), w_j) < \textsc{Agg}(F(\mathcal{P}[j]), w_j)$ **then**
            $\mathcal{P}[j] \leftarrow y$
          end if
        end for
      end for
    else ▷ $M = \text{GDE3}$
      $\mathcal{T} \leftarrow \textsc{MutateAndCrossover\_DE}(\mathcal{P})$; $\mathcal{U} \leftarrow \mathcal{P} \cup \mathcal{T}$
      Fronts $\leftarrow \textsc{FastNonDominatedSort}(\mathcal{U})$; $\mathcal{P} \leftarrow \textsc{TruncateByFrontsAndCrowding}(\text{Fronts}, P)$
    end if
    $\textsc{UpdateExternalArchiveIfUsed}()$
  end for
  $\mathcal{P}_s^\star \leftarrow \textsc{ExtractParetoFront}(\mathcal{P})$; Store $\mathcal{P}_s^\star$
end for
$\mathcal{P}^\star \leftarrow \textsc{AggregatePareto}(\{\mathcal{P}_s^\star\})$; $x^\circ \leftarrow \textsc{IdentifyKneePoint}(\mathcal{P}^\star)$
return $\mathcal{P}^\star$, x°, $\textsc{Metrics}(x^\circ)$

Knee point-guided capacity sizing for hybrid PV–small hydropower systems

Capacity planning for power systems that integrate variable renewable energy (VRE) sources such as solar PV and small hydropower is inherently an optimization challenge. Solving this problem requires not only identifying a set of Pareto-optimal solutions but also selecting the most suitable design from this set. This selection process is typically addressed using a posteriori decision-making method, where a trade-off solution is chosen after analyzing the optimization results. In the absence of explicit stakeholder preferences, system designers often focus on a narrow region of the Pareto front where marginal gains in one objective no longer justify significant sacrifices in the other. Solutions outside this region frequently lead to higher LCOE or reduced energy output, thereby reducing the economic and operational efficiency of the system. A well-established approach in multi-objective optimization literature for guiding such decisions is the solution on the Pareto front that offers the best compromise between conflicting objectives—typically the point of maximum marginal utility [64, 65]. In practical terms, it is the solution beyond which any further improvement in one objective leads to a disproportionate degradation in the other [66]. This makes the knee point an attractive and rational choice for system designers when no explicit preferences exist. In two-objective problems, the knee point can be geometrically defined as the point on the Pareto front that has the maximum perpendicular distance d from the linear segment (or hyperplane in higher dimensions) connecting the two extreme Pareto-optimal points, denoted as P_1 and P_2. This concept is illustrated in Fig. 3. Intuitively, the knee point Q captures the highest level of trade-off efficiency and serves as a robust guideline for the capacity sizing of hybrid PV–small hydropower systems.

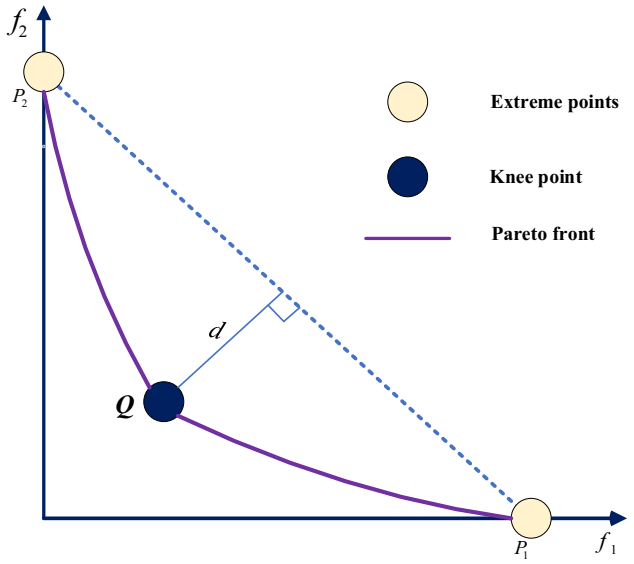

Fig. 3 Illustration of the knee-point approach in multi-objective optimization

The Pareto front quality was assessed based on non-dominated (ND) set size and hypervolume (HV) for a uniform reference across all multi-objective algorithms.

Case study description and simulation data

Case study description

This study proposes the hybridization of a small-hydro power plant with a solar PV plant, whereby the combined power output feeds the electrical loads along the power evacuation line (46 km, 33 kV) that interconnects with a 132/33 kV substation which is also connected to the national grid. A distribution network along the power evacuation route serves areas previously unserved by the national grid. The general layout is shown in Fig. 4. The 9 MW mini-hydro power plant under consideration is the Kabalega Hydromax Hydroelectric Power Station, which is located in Uganda (latitude: 01°32′42″ N, longitude: 31°06′41″ E, altitude: 964 m).

Simulation data

Long historical datasets are critical for hydrological studies. In [67], records from 1931–2004 underpin energy-availability modeling for small hydropower reliability, illustrating why extended inflow series are preferred. In [68], long-term daily streamflow was studied for the years 1951–2020 to undertake hydropower generation planning. For River Wambabya, we compiled daily average flows from Uganda's Directorate of Water Resources Management (DWRM) for 1970–1979 and from the generation plant records for 2015–2022. No observations exist for 1980–2014 because the gauge was destroyed during civil conflict.

To represent both long-term variability and recent changes in climate and catchment conditions, we analyze the periods separately and in combination. Minitab statistical software was used to preprocess the data and undertake statistical analyses. The mean of the river discharge for the dataset of 1970–1979 was 4.559 m^3/s while that for the dataset of 2015 to 2022 was 4.092 m^3/s. The inter-quartile range (IQR) of the river discharge for the dataset of 1970–1979 is 3.518 m^3/s while that for 2015–2022 is 3.376 m^3/s. The two values are within 4% of each other. When the impact of outliers is removed, the trimmed mean (Trmean) at 5% for the 1970 to 1979 dataset was 3.8619 m^3/s while that for 2015–2022 is 3.8204 m^3/s. The delta (Δ) = $TrMean_{2015-2022}/TrMean_{1979-1979} \approx 0.989$. Similarly, the trimmed mean at 10% is 3.660 m^3/s and 3.686 m^3/s for 1970–1979 and 2015–2022, respectively. The corresponding delta ≈ 1.007. This shows that the flows registered in the recent period are representative of the flows measured in the earlier period and thus validates the statistical comparability of the two periods.

We therefore constructed flow-duration curves (FDCs) for each period and for the combined series (1970–1979 + 2015–2022) as depicted in Fig. 5. The FDC depicts the probability of a given discharge being exceeded (which is percentage of time a given river discharge was equaled or exceeded over the entire period under consideration for all recorded discharges). The design discharge, Q_{design} is selected from the interquartile band (Q25–Q75) of the FDCs, which is consistent with hydropower practice that bases sizing on central FDC quantiles [68–71]. As a conservative choice, we adopted the lower FDC for sizing, giving $Q_{design} = 3.518$ m^3/s (based on the IQR). From the combined FDC, Q_{design} is placed at 49.56% exceedance and the shaded region corresponds to all flows that would ultimately contribute to power generation while adhering to the environmental flow (Q_{env}) which is 0.22 cumecs for River Wambabya. The stochastic representation employs a 3-parameter lognormal distribution fitted to the lower FDC (with scale, location and threshold parameters of 0.92587, 0.98356, and 0.43146, respectively), which we used to generate synthetic river discharge series of $n \times T$ years that was used in the optimization procedures. This approach captures long-term variability, reflects recent hydrologic changes, and yields a robust design discharge.

For solar irradiance data, a dataset of 25 years of hourly global solar irradiance data and ambient temperature for 1998–2022 was obtained from SOLARGIS [72]. Using the hydrological data obtained, the mean daily river flow data over a 365-days period and the daily average hourly global solar irradiance were processed and are presented in Figs. 6 and 7, respectively. These graphs align with the fact that

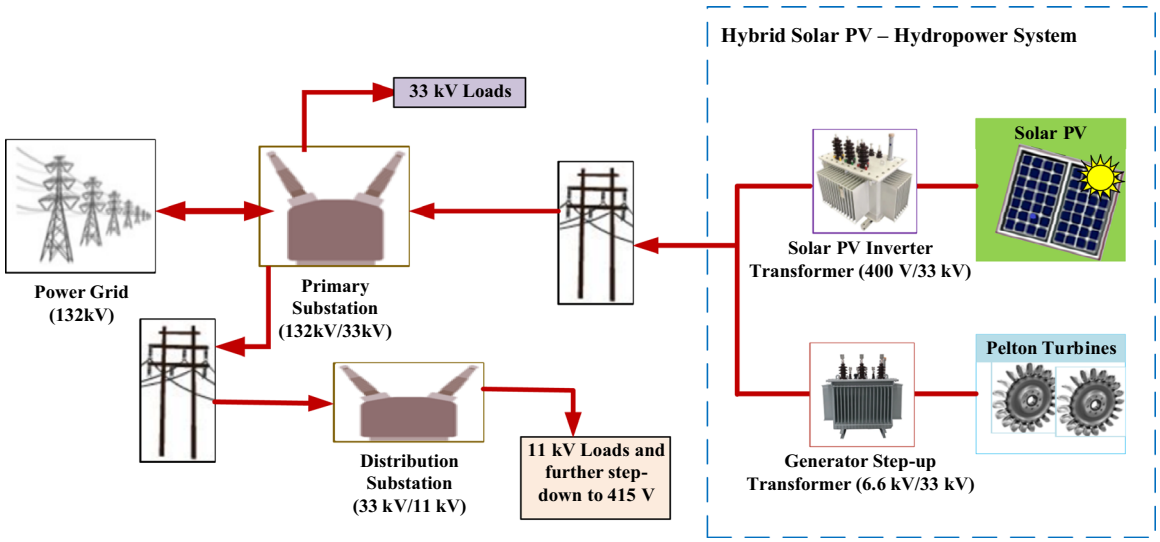

Fig. 4 Schematic of the hybrid solar PV-SHPP

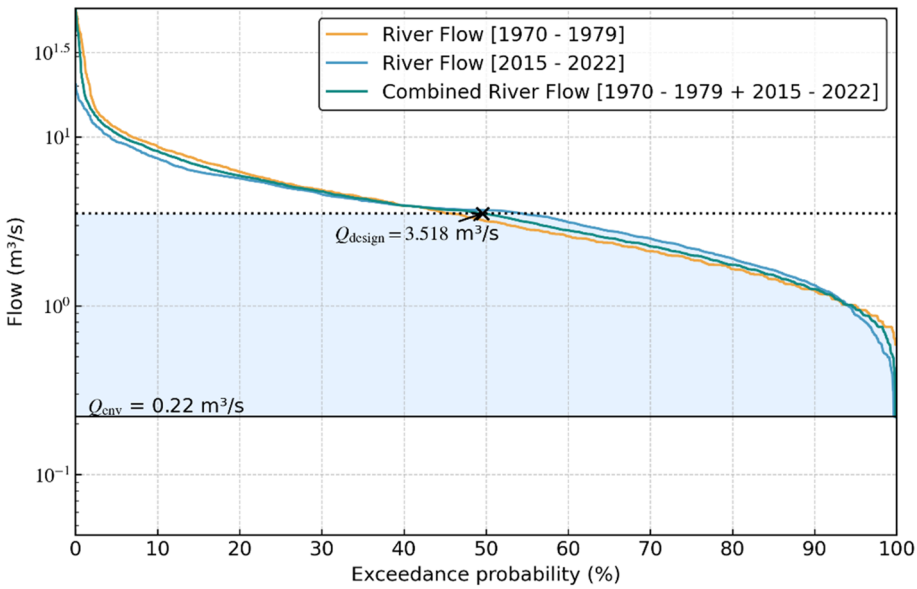

Fig. 5 Flow duration curves based on River Wambabya actual discharges for the period 1970–1979 and 2015–2022. A base 10 logarithmic scale is used for the y axis

Uganda has two dry and two wet seasons. The dry seasons are experienced in the months of December to February and June to August, while the months of March to May and September to November represent the wet seasons. Generally, December to February is hotter and drier whereas March to May is warmer and wetter.

Results and discussions

This section presents the results of applying multi-objective and single-objective approaches to solve the VRE capacity planning optimization problem. Our optimization procedure accounts for both internal and external uncertainties by considering the turbine efficiency specific to a particular turbined flow, as well as the uncertainty due to hydrological conditions, solar irradiance, and temperature. The end goal is three-fold: (a) to determine the appropriate capacity of a solar PV plant to be hybridized with the SHPP; (b) to determine the optimal number of turbines for the SHPP; and (c) to determine the optimal turbine flow for each turbine which aids in determining the turbine type and design discharge.

Performance comparison of multi-objective optimization algorithms

To evaluate the effectiveness of the multi-objective optimization algorithms applied in this study, a comparative analysis of their respective Pareto fronts was conducted under identical input and boundary conditions. All algorithms: namely,

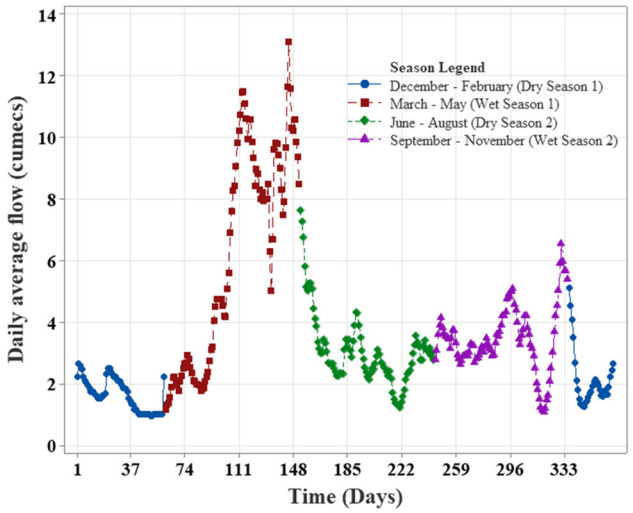

Fig. 6 Average daily flows for River Wambabya (1970–1979; 2015–2022)

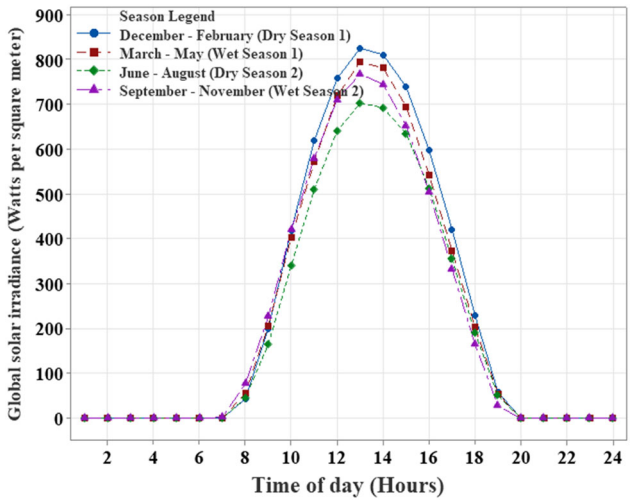

Fig. 7 Average hourly global solar irradiance for Buseruka (1998–2022)

NSGA-II, MOEAD and GDE3, were executed independently across 100 stochastic scenarios using the same cardinal input parameters. The resulting Pareto fronts were then aggregated and visualized in Fig. 8, representing the average performance envelope of each algorithm. The Pareto front generated by NSGA-II consistently lies closer to the origin of the objective space, indicating superior trade-off performance between the two conflicting objectives: maximizing total generated energy and minimizing energy production cost. In multi-objective optimization, proximity to the origin signifies more efficient solutions in both dimensions.

The Solar PV–hydro capacity optimization problem has non-convex, partially disconnected trade-offs and tight feasibility regions driven by hydrological and operational constraints. NSGA-II's elitist non-dominated sorting with crowding distance advances quickly into feasible regions while preserving spread especially around the knee where small cost increases yield large reliability gains. In contrast, MOEAD's fixed decomposition tends to oversample extremes and under-represent the mid-front solutions, and constraints further reduce the effectiveness of the scalar subproblems. GDE3's differential steps are efficient on smooth, unconstrained landscapes but, under binding constraints and repairs, tend to reduce effective step sizes near constraints yielding slightly lower front coverage.

To quantify computational efficiency and performance consistency, two stopping indicators were tracked for each algorithm: (i) the generation at which 95% of the best-seen hypervolume (HV) was first achieved (common "near-convergence" proxy), and (ii) the generation at which the non-dominated (ND) solutions/set size stabilized over a 20-generation window (adequate Pareto coverage). Using the same HV reference point (E = 482.94 GWh, Cost = 66.37 million US$) for all algorithms, NSGA-II and GDE3 both reached 95% HV by the 3rd generation and stabilized their ND sets by the 25th generation (final ND size = 100). MOAED achieved 95% HV in the first generation but required 65 generations to stabilize the ND set (final ND size = 101), reflecting slower coverage even though near optimal HV was achieved very early. The final and best attained HV values are shown in Table 4 below. NSGA-II yielded the highest HV, followed by GDE3 while MOEAD plateaued lower. These patterns match the ND-size and HV traces depicted in Figs. 9 and 10, respectively.

NSGA-II's dominance over other algorithms suggests its greater capability in identifying solutions that provide better economic and operational balance. To facilitate the final decision-making process, the knee point of the NSGA-II Pareto front was identified and utilized as the preferred solution. This point serves as a rational compromise and provides practical guidance for system designers in selecting an optimal configuration that ensures both cost-effectiveness and high energy yield. In contrast, the Pareto fronts obtained by both MOEAD and GDE3 were observed to be less competitive, particularly in regions of high energy output. These solutions tended to exhibit higher production costs for comparable energy levels and lacked the pronounced curvature necessary to define a strong knee point. This suggests that while the rest of the algorithms can explore the solution space, they may struggle with convergence and diversity maintenance in problems with highly non-convex or conflicting objective landscapes, as seen in hybrid VRE systems. The minimum, mean and maximum values for selected parameters for NSGA-II, MOEAD and GDE3 are presented in Tables 5, 6 and 7 respectively.

The knee point represents a levelized energy generated of 729.14 GWh and an energy production cost of US$ 47.66 million over the plant's design lifetime. The mean installed

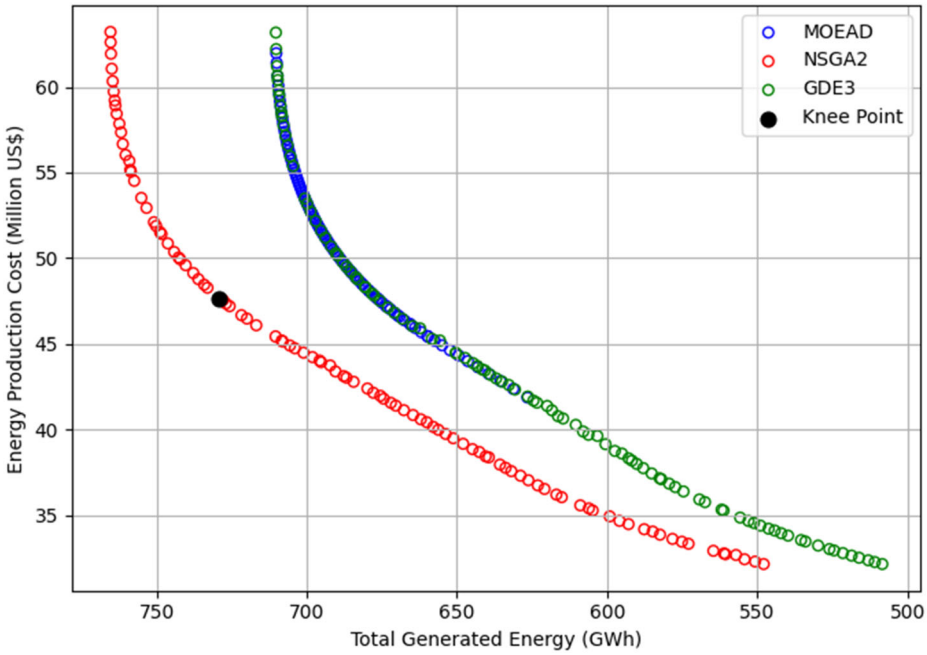

Fig. 8 Pareto graphs of the multi-objective algorithms at a discount rate of 11%

Table 4 Generations for 95% HV, stabilized ND-size, final ND size, final and maximum HV

Algorithm	Generation @ 95% HV	Generation for stabilized ND-size (window = 20)	Final ND size	Final HV	Max HV	Generation @ Max HV
NSGA-II	3	25	100	7715.47	7716.32	58
GDE3	3	25	100	5967.37	5973.14	171
MOEA/D	1	65	101	5082.60	5468.59	58

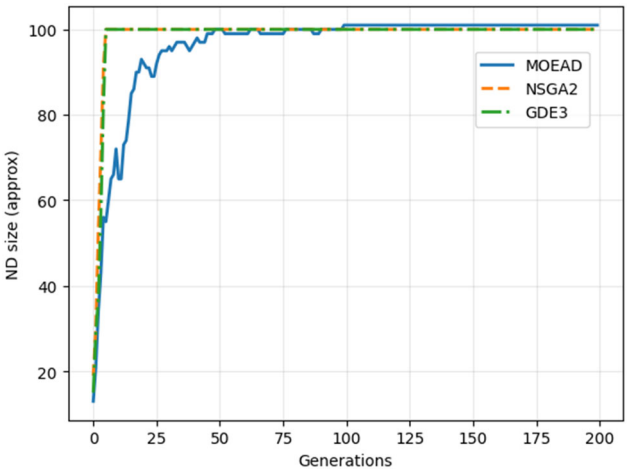

Fig. 9 Trace of the non-dominated size over the number of generations for the multi-objective algorithms

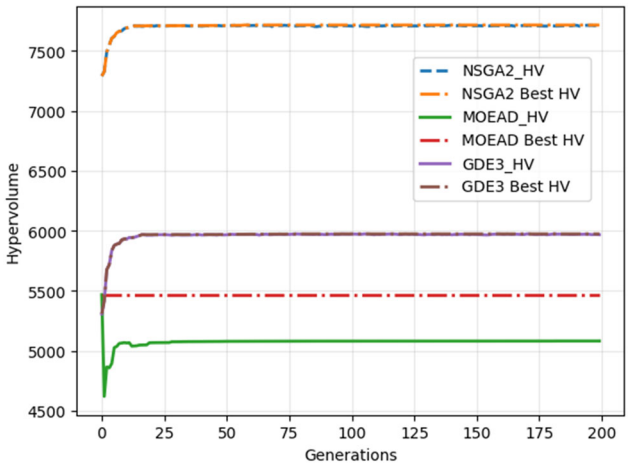

Fig. 10 Trace of hypervolume over the number of generations for the multi-objective algorithms

discharge per turbine is 1.18 m^3/s which closely matches the actual design discharge for the Pelton turbines installed at the plant which is 1.12 m^3/s. Based on the knee point, we selected the installed capacity of the hydropower plant to be 6.33 MW which is hybridized with a solar PV plant of 10.00 MWp since the capacity factor for Solar PV is approximately 19.73% irrespective of the installed capacity. The corresponding capacity for the hybrid Solar PV-SHPP is 16.33 MW with a capacity factor of 42.74% and a LCOE of US ¢ 6.54/kWh.

Table 5 Optimized LCOE and corresponding plant parameters for NSGA-II

Parameter description	Minimum	Mean	Maximum	Knee point
Levelized generated energy (GWh)	545.19	674.58	759.42	729.14
Levelized energy production cost (million USD)	32.14	44.36	63.19	47.66
Capacity of the solar PV plant (MWp)	5.00	7.87	10.00	10.00
Installed discharge for the SHPP (m^3/s)	0.895	1.11	1.56	1.18
Number of turbines	2	2	3	2
Capacity of the SHPP (MW)	4.80	5.96	9.39	6.33
Capacity factor for hydro (%)	69.45	79.13	85.24	83.12
Capacity factor for solar (%)	19.73	19.73	19.73	19.73
Capacity factor-hybrid solar PV-SHPP (%)	42.44	47.43	53.34	42.74
LCOE (US ¢/kWh)	5.89	6.58	8.32	6.54

Table 6 Optimized LCOE and corresponding plant parameters for MOEAD

Parameter description	Minimum	Mean	Maximum
Levelized generated energy (GWh)	626.53	687.29	710.14
Levelized energy production cost (Million USD)	41.88	51.23	61.97
Capacity of the solar PV plant (MWp)	7.94	9.90	10.00
Installed discharge for the SHPP (m^3/s)	1.04	1.26	1,19
Number of turbines	2	2	3
Capacity of the SHPP (MW)	5.74	7.03	9.11
Capacity factor for hydro (%)	70.03	77.05	82.13
Capacity factor for solar (%)	19.71	19.72	19.70
Capacity factor-hybrid solar PV-SHPP (%)	43.14	44.43	46.12
LCOE (US ¢/kWh)	6.68	7.45	8.72

Table 7 Optimized LCOE and corresponding plant parameters for GDE3

Parameter description	Minimum	Mean	Maximum
Levelized generated energy (GWh)	506.76	628.33	708.06
Levelized energy production cost (million USD)	32.14	43.97	63.18
Capacity of the solar PV plant (MWp)	5.00	7.90	10.00
Installed discharge for the SHPP (m^3/s)	0.895	1.18	1.26
Number of turbines	2	2	3
Capacity of the SHPP (MW)	4.80	6.32	9.39
Capacity factor for hydro (%)	69.36	80.44	85.22
Capacity factor for solar (%)	19.70	19.71	19.72
Capacity factor-hybrid solar PV-SHPP (%)	42.15	47.26	53.34
LCOE (US ¢/kWh)	6.34	7.00	8.92

Table 8 Plant/capacity factors for Kabalega/Hydromax SHPP

Year	2019	2020	2021	2022	2023	Average
Energy (MWh)	50,506	78,401	67,319	54,335	65,046	63,121
Capacity factor (%)	64.06%	99.44%	85.39%	68.92%	82.50%	80.06%

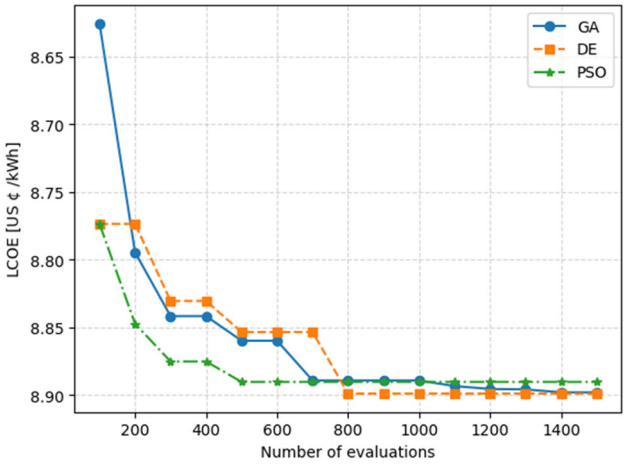

Fig. 11 Convergence plot of the single objective algorithms

The average capacity factor of the 9 MW Kabalega Hydromax HPP based on real operation data for the years 2019–2023 was calculated to be 80% as shown in Table 8. Based on our simulation, the capacity factor ranged from 69.36 to 85.24% with a mean of 79.13% which depicts a robust optimization model that caters for the variability in the plant's power output over its life cycle.

For all the simulation scenarios, the solar PV plant capacity factor was determined to range from 19.71 to 19.83%. This shows an improvement compared to the study presented in [73], where four grid-connected solar PV plants were studied and the capacity factors based on actual generation data were determined to be 13.1, 13.7, 17.5 and 17.5% respectively.

Performance comparison of single-objective optimization algorithms

The single-objective function was set up using Eq. (3) which is essentially a minimization of the LCOE for the hybrid power system. The convergence of GA, DE and PSO for 1,500 function evaluations is depicted in Fig. 11 below. PSO showed the fastest convergence followed by DE while GA required the most function evaluations to achieve convergence. Table 9 presents the corresponding results after conducting simulations based on the proposed framework.

Additionally, the statistical evaluation of the single-objective optimization algorithms is presented in Table 10, which summarizes the performance of each method over 100 independent simulation scenarios. The table reports key metrics of the LCOE, including the mean, standard deviation, minimum, and maximum values for each algorithm. The results demonstrate that DE outperforms the other methods in terms of overall cost-effectiveness. However, its performance doesn't significantly differ from the other single-objective algorithms statistically. DE achieved the lowest average LCOE of US ¢ 8.96, indicating superior long-term economic performance. It also exhibited the lowest maximum LCOE of US ¢ 9.02, suggesting more favorable worst-case outcomes compared to PSO and GA. Moreover, DE maintained a slightly lower standard deviation, reflecting consistent performance across all scenarios. PSO exhibited slightly higher variability, implying less reliability in reaching consistently optimal solutions. GA displayed performance similar to that of DE in terms of stability, but with a slightly higher average and maximum LCOE. Overall, DE strikes the best balance between optimization quality and consistency, making it the most reliable algorithm for minimizing the LCOE in single-objective capacity planning of hybrid PV–small hydropower systems.

Sensitivity analysis

The major drivers of LCOE are usually initial capital cost and capacity factors. Furthermore, in the optimization of the LCOE, the weighted average cost of capital (WACC)/discount rate, directly reshapes the objective function by re-weighting early capital expenditure (CAPEX)

Table 9 Optimized LCOE and corresponding plant parameters for single-objective algorithms

Parameter description	GA	DE	PSO
Levelized generated energy (GWh)	701.87	704.69	702.88
Levelized energy production cost (million USD)	62.93	63.16	63.03
Capacity of the solar PV plant (MWp)	9.84	9.97	9.89
Installed discharge for the SHPP (m^3/s)	1.17	1.16	1.17
Number of turbines	3	3	3
Capacity of the SHPP (MW)	9.4	9.4	9.4
Capacity factor for SHPP (%)	80.76	80.63	80.58
Capacity factor for solar PV (%)	19.76	19.79	19.80
Capacity factor-hybrid solar PV-SHPP (%)	49.56	49.31	49.40
LCOE (US ¢/kWh)	8.97	8.96	8.97

Table 10 Statistical analysis of single-objective algorithms' performance based on LCOE (US ¢)

Algorithm	Mean	Std	Minimum	Maximum
PSO	8.97	0.05	8.88	9.04
DE	8.96	0.04	8.86	9.02
GA	8.97	0.04	8.87	9.03

against future operations and maintenance (O&M) and energy revenues; as a result, the optimal design may vary with the discount rate. To cover concessional/low-risk, Uganda's benchmark of 11%, and high-risk financing, we test 7%–11%–15%. At 7%, capital-intensive, long-lived options become cheaper in present-value terms, frequently moving the optimizer toward larger or earlier PV–small hydro–storage projects and often a lower LCOE. At 15%, the aim penalizes upfront CAPEX, preferring shorter-payback or higher utilization choices and delaying additions usually reflected by a higher LCOE.

Based on this variation, the multi-objective algorithms yielded mean LCOE values of US ¢ 5.70/kWh and US ¢ 8.72/kWh for discount rates of 7 and 15% respectively. Similarly, the single-objective algorithms yielded mean LCOE values of US ¢ 7.07/kWh and US ¢ 10.89/kWh for discount rates of 7% and 15% respectively. The knee point values for the 7% discount rate are a LCOE of US ¢ 5.55/kWh and 932.58 GWh being the levelized generated energy. For the 15% case, the knee point values are a LCOE of US ¢ 8.65/kWh and 519.43 GWh being levelized generated energy over the design life of 25 years. This sensitivity measures finance-driven uncertainty, verifies design stability and shows that the proposed framework is robust under realistic capital-market circumstances, with 11% serving as the primary case.

As indicated in Tables 5, 6, 7 and 9, the solutions obtained using the multi-objective optimization algorithms had the optimal number of turbines being either 2 or 3, while all the single-objective algorithms had the optimal number of turbines being 3. Using multi-objective algorithms, the nominal/rated turbine discharge corresponding to 2 and 3 turbines for each of the 100 points on the Pareto front of the NSGA-II algorithm was separately mapped out along with the associated energy generated and its production cost. The capacity factor was calculated using the energy generated in relation to the obtained installed capacities of the small hydropower plant. Using this data, the impact of the number of turbines and nominal turbine discharge on the energy production, capacity factor of the hydropower plant and energy production costs was evaluated. The results are shown on Figs. 12, 13 and 14, respectively. As expected, the energy generated, and energy production costs are higher for $n_{hyd} = 3$ than for $n_{hyd} = 2$ and increase with the increase in the discharge. However, the capacity factor of the hydropower power plant

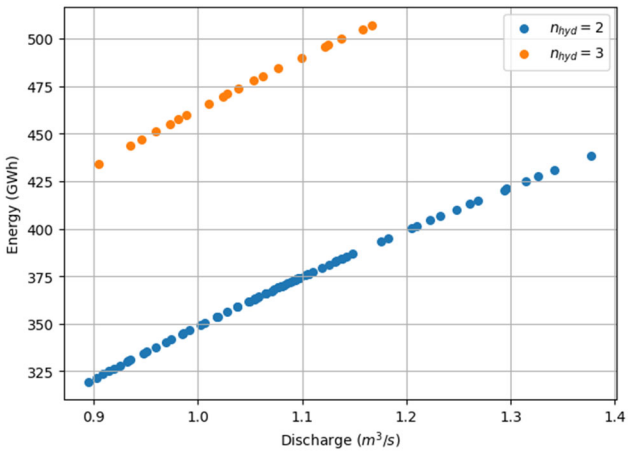

Fig. 12 Variation of energy generated with discharge and number of turbines

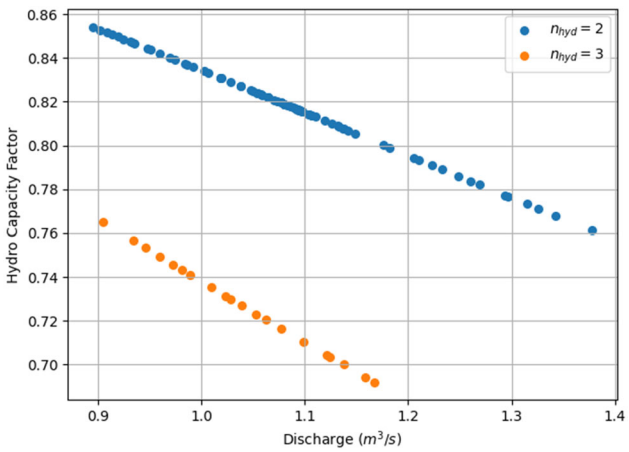

Fig. 13 Variation of hydropower plant capacity factor with discharge and number of turbines

decreases with an increase in discharge and is less for $n_{hyd}=3$ than for $n_{hyd} = 2$.

The plots explain why the multi-objective optimization algorithms sometimes select $n_{hyd} = 2$ whereas the single-objective LCOE runs converge to $n_{hyd} = 3$. For each NSGA-II pareto point, mapping rated turbine discharge with energy, cost, and capacity factor shows a clear trade-off: increasing Q_{Tr} and or moving to three turbines raises annual energy but also raises production costs, while capacity factor declines because installed capacity increases faster than the energy generated under the site's river discharge/flow regime.

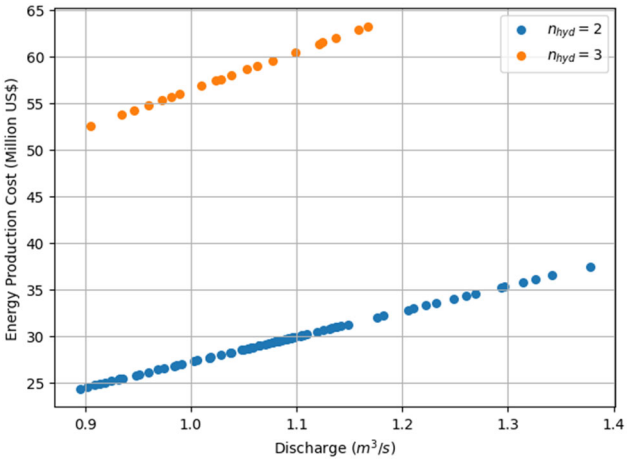

Fig. 14 Variation of energy production cost with discharge and number of turbines

Consequently, the Pareto front reveals diminishing returns in energy versus cost and a utilization capacity penalty at higher Q_{Tr} and n_{hyd}. The plots therefore justify the presence of two variable optima: (i) lower cost, higher-capacity factor designs with two turbines and moderate Q_{Tr}, and (ii) higher generation, higher cost designs with three turbines, and demonstrate that the selected configuration is a transparent, data-driven trade-off.

Comparative analysis with existing methods and other hybrid/renewable energy systems

This section presents a comprehensive comparative analysis and performance evaluation of the optimization algorithms applied to enhance the design and operational efficiency of a hybrid solar PV–small hydropower system. The focus is on the optimal configuration of key system components, including the number of hydropower turbines, the total number of photovoltaic modules, and the design discharge rate. The optimization was carried out using six evolutionary algorithms: GA, PSO and DE for single-objective optimization and the NSGA-II, GDE3, and MOEAD for multi-objective optimization. The primary objective of this evaluation is to assess the effectiveness of these algorithms in determining design parameters that maximize power output, ensure seamless grid integration, and promote stable and reliable operation under varying environmental conditions. For the base discount rate of 11%, NSGA-II demonstrated superior performance for the hybridized plant, achieving an optimal LCOE of US ¢ 6.54/kWh US cents per kWh and a capacity factor of 42.74% at the knee point. These results indicate that NSGA-II effectively leveraged the complementary nature of solar and hydro resources to maximize energy yield and minimize lifecycle costs. In contrast, while the DE algorithm also produced economically viable and technically sound configurations, its performance in terms of both LCOE and capacity factor was slightly lower than that of NSGA-II. The findings underscore the critical role of advanced optimization techniques in the design and planning of hybrid renewable energy systems. By enabling efficient sizing and integration of system components, these algorithms help mitigate the challenges posed by seasonal variability and intermittency, ultimately leading to more resilient and cost-effective power systems.

Compared with other approaches in the literature, the results of this study reveal the robustness of the proposed methodology. For example, in [74], HOMER was used to undertake a pre-feasibility economic and sensitivity assessment of a Hybrid Renewable Energy System and the resulting minimum cost of energy was US ¢ 19.6 per kWh which is more than double the optimized levelized cost of electricity obtained in this study. The LCOE from this study also outperforms the multi-objective sizing optimization using the particle swarm optimization approach presented in [25] where the optimization was focused on sizing a hybrid renewable energy system that minimized the LCOE and Loss of Power Supply Probability (LPSP) and the resulting LCOE range was from USD 118.6/MWh to 229.7/MWh (which is equivalent to about US ¢ 10.72 to US ¢ 22.97 per kWh). Furthermore, the global weighted average capacity factors for utility scale solar PV ranges from 10 to 21.7% at the 5th and 95th percentiles while that of small hydros ranged from 30 to 75% [41]. The capacity factors for the hybrid system obtained in this study ranged from 42.44 to 53.34% which are within the published capacity factors for hybrid solar PV–small hydro power systems which typically range from 40 to 60% as the two resources complement each other.

Alignment with policy/tariff frameworks and adoption cost margins

The LCOE values obtained for both single and multi-objective algorithms are within the range of the average of US ¢ 10.3/kWh for the existing/operational solar PV and SHPP in Uganda as of December 2024 which informed our study's tariff cap due to hybridization of an existing run-of-river plant. It is important to note that in August 2023, the Electricity Regulatory Authority (ERA) of Uganda published new renewable energy feed-in-tariffs (REFIT), Phase VI [75]. Under REFIT Phase VI, the FIT for a 9 MW small hydropower is US ¢ 7.52/kWh while that for Solar PV up to 20MWp was US ¢ 7.1/kWh, respectively. However, effective April 2025, ERA reduced the standardized Solar PV tariff to US ¢ 5.1/kWh for capacities of 0.5 to 50 MW; small hydropower tariffs follow a size dependent linear schedule of US ¢ 7.92 → 6.22/kWh for 5 to 50 MW [76]. For our hybridized plant, the applicable tariff would be US ¢

5.1/kWh for the 10MWp Solar PV and US ¢ 7.79/kWh for the 6.33 MW hydro. From this study, using the optimal installed capacities of 10MWp Solar PV and 6.33 MW for hydro with capacity factors of 19.73% and 70% (taking the conservative lowest capacity factor for hydro) respectively, the energy weighted average tariff for the hybridized plant is US ¢ 6.96/kWh with solar PV contributing about 30.8% of the total generated energy compared to 69.2% by hydro.

Furthermore, the values of LCOE obtained from this study are within the range of the latest global LCOE of solar and small hydropower projects as reported by the International Renewable Energy Agency (IRENA). For 2023, IRENA reported the LCOE for utility scale solar power plants to range from approximately US ¢ 3.2/kWh to approximately US ¢ 11.5 per kWh at the 5th and 95th percentile, respectively while the LCOE for small hydropower plants was reported to range from about US ¢ 6.2 to US ¢ 14.9/kWh at the 5th and 95th percentiles, respectively [41]. Regionally, recent auctions in sub-Saharan Africa have yielded solar PV tariffs that are below Uganda's historical FIT mainly because they combine lower effective WACC via concessional/debt from Development Financing Institutions (DFIs), partial risk guarantees, and hedging of foreign exchange. This is augmented by declining equipment costs (global PV CAPEX/LCOE downtrends) and use of standardized, bankable PPAs with sovereign support, grid-ready sites and land provided by the regulators/host Country, and scale and competitive auctions that sharpen price discovery. Table 11 below shows the tariffs for utility-scale Solar PV projects [77–83] across Sub-Saharan Africa.

Adoption cost margins At the base discount rate of 11%, the optimal tariff for the hybridized plant was US ¢ 6.54/kWh at the knee, providing a cost margin of + US ¢ 0.42/kWh when compared to the applicable weighted average energy tariff of US ¢ 6.96/kWh. At 7% discount rate, this margin increases to + US ¢ 1.46/kWh since the optimal tariff at the knee is ≈ US ¢ 5.5/kWh. The implication is that the solutions arising from the proposed framework are competitive considering the current trend where financing terms are likely to approach regional auction norms (which usually benefit from lower WACC/concessional financing), and PV/Battery Energy Storage Systems (BESS)' CAPEX continues to decline [41].

Considering the above results, it is certain that as the cost of capital goes down, and the discount rates decline (due to concessional and climate financing among other factors), the revised ERA's REFIT can be achieved without any need for Government subsidies. In addition, given regional evidence that competitive tenders routinely clear at ≤ US ¢ 4/kWh when coupled with concessional financing and standardized PPAs, Uganda should prioritize competitive auctions to support transparent price discovery and optimally allocate the

Table 11 Regional/Sub-Saharan Africa auction/PPA benchmarks for utility-scale solar PV

Country	Mechanism	Project/program	Award year	Capacity (MW)	Tariff (US ¢/kWh)
Uganda	REFIT (historical & revised)	REFIT phase VI April 2025 revision	2023/2025	≤ 50	7.1 (historical) 5.1 (revised–April 2025)
Tunisia	Auction/National tender	500 MW and Tataouine 200 MW	2019	700	≈ 2.44–3.01
Kenya	FIT (legacy) → auction/negotiated PPA	Garissa solar PV	2018–2019 PPA revision	54.6	5.49
Egypt	Auction/IPP (DFI-backed)	Abydos solar	2022	560	≈ 2.0
South Africa	Auction REIPPPP-BW6	REIPPPP BW6 (solar awards)	2022	≈ 860	≈ 2.8–3.0
Zambia	GET FiT Auction	GET FiT Zambia solar	2019	120 (multiple 20 MWac)	3.99 (low) 4.41 (average)
Senegal	Auction (scaling Solar)	Kahone & Kael	2018–2019	60	≈ 4.1–4.4

scarce grid capacity. Our optimization framework would simply replace the FIT cap with the current/reference auction clearing price as the affordability constraint.

Application of the proposed framework in real-world deployments

Utility planners, regulators, independent power producers/developers, policy makers and financiers usually rely on feasibility studies to determine project bankability. The feasibility studies support this analysis by sizing the plant capacity, quantifying costs, and checking compliance with tariffs and grid codes. Our stochastic optimization framework turns this process into a repeatable workflow that adheres to feed-in tariffs (FITs), WACC/discount rates, environmental constraints, as well as declining CAPEX for solar and storage as may be required. It is applicable to greenfield VRE-based projects and retrofits of run-of-river plants. The main steps in applying the framework include:

1) Identifying the resource and building realistic uncertainty data sets

Action: For hydropower, compile multi-decade river flows (daily/weekly) including drought percentiles from the flow duration curve (FDC). For solar, use multi-year hourly irradiance (GHI/POA) to capture interannual variability. Clean data and check for bias; generate ensembles via bootstrapping/Monte Carlo.

Output: A scenario pack (for example., $\geq$ 100 weather–demand traces) to be used in optimization.

2) Fixing policy, regulatory and finance metrics

Action: Treat published FITs/tariff ceilings as hard constraints. Set the WACC/discount rate per the regulator and test Low/Base/High cases (± 2 to 5%). Encode compliance constraints: environmental flows, ramp-rate limits, curtailment caps, minimum firm capacity, and any power purchase agreement (PPA)/grid-code conditions. Align CAPEX/OPEX with current benchmarks.

Output: A *"constraints list"* with numeric bounds and financing parameters.

3) Setting and executing the optimization procedures

Action: Set-up the optimization procedures as detailed under "Solution approach" in this paper. NSGA-II is the proposed default algorithm, and cross-checks can be made with the others. Appropriate parameter settings and seeds must be well documented, and convergence tracked. Stress test candidate solutions and run sensitivity checks and screening for affordability and finance robustness.

Output: Decision artifacts such as a Pareto front with knee-point call outs and trade-off tables of levelized costs, levelized generated energy, capacity factors, number of units, etc. Planners select the most robust option that best meets all the set constraints.

4) Grid integration checks and commercial structuring

Action: Run grid-integration checks (power-flow/short-circuit analysis) and necessary iterations for sizing made to confirm the most optimal designs. Use results to inform PPA negotiation and licensing processes, confirming bankability pathways and financial structuring.

Output: Grid-validated candidate designs with clear interconnection implications; project license and achievement of financial close.

5) Project execution and monitoring and periodic refresh

Action: Continue monitoring and recording irradiance, hydrology and other key data; update dispatch and planning runs quarterly.

Output: Living models and auditable reports for policy makers, regulators, lenders and operators.

The framework therefore operationalizes stochastic optimization for planners and financiers. It enforces FIT and grid compliance, prices risk via WACC scenarios and delivers a set of build-ready, regulator-compliant portfolio that advances sustainable capacity planning for VRE based projects.

Conclusion and future work

This study proposed a robust modelling, simulation and optimization framework for the capacity planning of hybrid power plants that rely on variable renewable energy (VRE) resources. The methodology employed six metaheuristic algorithms: NSGA-II, MOEAD, and GDE3 for multi-objective optimization; and PSO, DE, and GA for single-objective optimization. The goal was to determine the optimal configuration of critical system components, including the number of PV modules, turbine units, and design flow rate. The multi-objective optimization aimed at the simultaneous maximization of total energy output and minimization of energy production cost, while single-objective optimization focused on minimizing the LCOE. A knee point detection method was applied to identify the most balanced solution along the Pareto front of the best-performing multi-objective algorithm, enabling informed decision-making in scenarios with competing objectives. Comparative performance analysis revealed that NSGA-II consistently yielded superior solutions, achieving the lowest LCOE and highest

capacity factor among the multi-objective methods. Similarly, DE outperformed other single-objective algorithms in terms of both accuracy and robustness across multiple stochastic scenarios. The proposed framework proves practical and scalable for renewable energy systems operating under climatic uncertainty, capital and tariff constraints. The results underscore the critical role of advanced optimization techniques in the design and long-term planning of hybrid renewable energy systems, offering valuable guidance to system developers, engineers, and policymakers committed to accelerating the clean energy transition.

This study focused on the capacity planning of the hybrid solar PV–SHPP with the goal of minimizing the levelized cost of electricity over the hybrid plant's lifecycle. The aspects of optimal operation and dispatch scheduling have not been analyzed, and this is a key area for future work. In addition, the key aspects of power system reliability, security and quality of supply, among others, were not assessed.

It will also be pertinent to analyze ramp rate aspects in subsequent studies as this is a key element that many power system operators continue to grapple with. With advances in forecasting, power plant operators can schedule and declare the available generation taking into consideration the forecasted variance in power output. For a hybrid solar PV–SHPP, the hydropower component can compensate for the errors in forecasting solar irradiance owing to the fast ramp-up exhibited by hydropower plants which is typically in the range of 10 to 30% [48]. This would augment the required plant and grid flexibility thereby minimizing the requirement for external ramp-up resources in dealing with the variations in Solar PV power output.

Acknowledgements We thank the Ministry of Energy and Mineral Development, Uganda, for sharing information on Uganda's energy sector. In addition, we extend our gratitude to the staff at Hydromax Limited, the developer of the 9 MW Kabalega Hydroelectric Power Station for sharing the data pertaining to the plant's feasibility study and operations. Finally, we acknowledge Solargis for providing solar irradiance and temperature data used in this study.

Author contributions Edward B. Ssekulima: Conceptualization, Methodology, Writing—original draft. Amir Etemadi: Writing—review & editing.

Data availability The data supporting the findings of this study will be available upon request.

Declarations

Conflict of interest The authors have no competing interests.

References

1. Andrean G, Bermudez JM, Budinis S, Collina L et al (2024) Energy technology perspectives 2024. International Energy Agency (IEA), Paris. https://www.iea.org/reports/energy-technology-perspectives-2024. Accessed 29 Aug 2025
2. IRENA (2025) Renewable power generation costs in 2024. International Renewable Energy Agency, Abu Dhabi
3. Masson G, de l'Epine M, Kaizuka I (2024) Trends in photovoltaic applications 2024. IEA PVPS Task 1, International Energy Agency Photovoltaic Power Systems Programme. https://doi.org/10.69766/JNEW6916 (**ISBN 978-3-907281-68-0**)
4. International Energy Agency (IEA) (2024) World Energy Outlook 2024. IEA, Paris. https://www.iea.org/reports/world-energy-outlook-2024. Accessed 28 Aug 2025
5. Sareen K, Panigrahi BK, Nagdeve R et al (2025) Energy transition: a global review of wholesale energy markets and variable renewable energy forecasting-related frameworks. IEEE Power Energy Mag 23:53–64. https://doi.org/10.1109/MPE.2025.3542765
6. Intergovernmental Panel on Climate Change (IPCC) (2023) Climate change 2023: the physical science basis. Intergovernmental Panel on Climate Change. https://report.ipcc.ch/ar6syr/pdf/IPCC_AR6_SYR_LongerReport.pdf. Accessed 4 May 2023
7. Erdiwansyah M, Husin H et al (2021) A critical review of the integration of renewable energy sources with various technologies. Prot Control Mod Power Syst 6:3. https://doi.org/10.1186/s41601-021-00181-3
8. Denholm P, O'Connell M, Brinkman G, Jorgenson J (2015) Overgeneration from solar energy in California. A field guide to the duck chart. National Renewable Energy Laboratory, Golden. NREL/TP-6A20-65023. https://doi.org/10.2172/1226167
9. Leone G, Catani V, Pagnozzi M et al (2023) Hydrological features of Matese Karst Massif, focused on endorheic areas, dolines and hydroelectric exploitation. J Maps 19:2144497. https://doi.org/10.1080/17445647.2022.2144497
10. Palmintier B, Broderick R, Mather B et al (2016) On the path to SunShot: emerging issues and challenges in integrating solar with the distribution system. National Renewable Energy Laboratory (NREL), Golden
11. International Energy Agency (2021) Technology collaboration programme on energy storage (ES TCP): annual report, 2021
12. Katz J, Chernyakhovskiy I (2020) Variable renewable energy grid integration studies: a guidebook for practitioners. National Renewable Energy Laboratory
13. Zandi H, Starke M, Winstead C et al (2023) Optimal operation of integrated PV and energy storage considering multiple operational modes with a real-world case study. IEEE Access 11:99070–99082. https://doi.org/10.1109/ACCESS.2023.3313502
14. Lund H (2014) Renewable energy systems—2nd edition. https://www.elsevier.com/books/renewable-energy-systems/lund/978-0-12-410423-5. Accessed 4 May 2023
15. ESMAP (Energy Sector Management Assistance Program) (2019) Grid integration requirements for variable renewable energy—technical guide

16. Zhou A, Yang M, Fang X, Zhang Y (2024) Addressing wind power forecast errors in day-ahead pricing with energy storage systems: a distributionally robust joint chance-constrained approach. IEEE Trans Sustain Energy 15:1754–1767. https://doi.org/10.1109/TSTE.2024.3374212
17. Hodge B-M, Brancucci Martinez-Anido C, Wang Q et al (2018) The combined value of wind and solar power forecasting improvements and electricity storage. Appl Energy 214:1–15. https://doi.org/10.1016/j.apenergy.2017.12.120
18. Zang H, Cheng L, Ding T et al (2018) Hybrid method for short-term photovoltaic power forecasting based on deep convolutional neural network. IET Gener Transm Distrib 12:4557–4567. https://doi.org/10.1049/iet-gtd.2018.5847
19. Razavi SE, Arefi A, Ledwich G et al (2020) From load to net energy forecasting: short-term residential forecasting for the blend of load and PV behind the meter. IEEE Access 8:224343–224353. https://doi.org/10.1109/ACCESS.2020.3044307
20. Guo X, Wang X, Ao Y et al (2022) Short-term photovoltaic power forecasting with adaptive stochastic configuration network ensemble. WIREs Data Min Knowl Discov 12:e1477. https://doi.org/10.1002/widm.1477
21. International Renewable Energy Agency (2018) Power system flexibility for the energy transition, Part 1: overview for policy makers
22. Kumar K, Jaipal B (2022) The role of energy storage with renewable electricity generation. In: Ghofrani M (ed) Electric grid modernization. IntechOpen
23. IRENA (2020) Electricity storage valuation framework—assessing system value and ensuring project viability. International Renewable Energy Agency IRENA, Abu Dhabi
24. Shafiullah G, Masola T, Samu R et al (2021) Prospects of hybrid renewable energy-based power system: a case study, post analysis of Chipendeke micro-hydro, Zimbabwe. IEEE Access 9:73433–73452. https://doi.org/10.1109/ACCESS.2021.3078713
25. Guo S, Kurban A, He Y et al (2023) Multi-objective sizing of solar-wind-hydro hybrid power system with doubled energy storages under optimal coordinated operational strategy. CSEE J Power Energy Syst 9:2144–2155. https://doi.org/10.17775/CSEEJPES.2021.00190
26. Roy P, He J, Zhao T, Singh YV (2022) Recent advances of wind-solar hybrid renewable energy systems for power generation: a review. IEEE Open J Ind Electron Soc 3:81–104. https://doi.org/10.1109/OJIES.2022.3144093
27. Rangel-Martinez D, Nigam KDP, Ricardez-Sandoval LA (2021) Machine learning on sustainable energy: a review and outlook on renewable energy systems, catalysis, smart grid and energy storage. Chem Eng Res Des 174:414–441. https://doi.org/10.1016/j.cherd.2021.08.013
28. Starke AR, Cardemil JM, Escobar R, Colle S (2018) Multi-objective optimization of hybrid CSP+PV system using genetic algorithm. Energy 147:490–503. https://doi.org/10.1016/j.energy.2017.12.116
29. Tsuanyo D, Amougou B, Aziz A et al (2023) Design models for small run-of-river hydropower plants: a review. Sustain Energy Res 10:3. https://doi.org/10.1186/s40807-023-00072-1
30. Voros NG, Kiranoudis CT, Maroulis ZB (2000) Short-cut design of small hydroelectric plants. Renew Energy 19(4):545–563. https://doi.org/10.1016/S0960-1481(99)00083-X
31. Ministry of Finance, Planning and Economic Development (MoFPED) Uganda National Parameters. https://national-parameters.ug/index.php?r=tradable%2Flist-parameters. Accessed 30 May 2023
32. Maxeon Solar Technologies (2022) Maxeon 6 solar panel (SPR-MAX6-420/425/435/440)—technical datasheet. Rev. A (A4_EN)
33. Mamo G, Marence M, Chacon-Hurtado J, Franca M (2018) Optimization of run-of-river hydropower plant capacity. International Water Power and Dam Construction
34. Sakki GK, Tsoukalas I, Kossieris P et al (2022) Stochastic simulation-optimization framework for the design and assessment of renewable energy systems under uncertainty. Renew Sustain Energy Rev 168:112886. https://doi.org/10.1016/j.rser.2022.112886
35. Fetio Ngoune N, Kanouo Djousse BM, Djoukeng GH et al (2023) Contribution of the mix renewable energy potentials in delivering parts of the electric energy needs in the west region of Cameroon. Heliyon 9:e14554. https://doi.org/10.1016/j.heliyon.2023.e14554
36. Koko SP, Kusakana K, Vermaak HJ (2018) Optimal sizing of a micro-hydrokinetic pumped-hydro-storage hybrid system for different demand sectors. Sustainable cloud and energy services. Springer, Cham, pp 219–242
37. Oladosu G, Sasthav C (2021) Hydropower capital and O&M costs: an exploration of the FERC form1 data. (ORNL/TM-2021/2297)
38. Aoun N (2024) Energy and exergy analysis of a 20-MW grid-connected PV plant operating under harsh climatic conditions. Clean Energy 8:281–296. https://doi.org/10.1093/ce/zkad088
39. Bentouba S, Bourouis M, Zioui N et al (2021) Performance assessment of a 20 MW photovoltaic power plant in a hot climate using real data and simulation tools. Energy Rep 7:7297–7314. https://doi.org/10.1016/j.egyr.2021.10.082
40. Benelkadi AO, Kaabeche A, Bakelli Y (2018) Technical and economic feasibility study of photovoltaic power plants in Algeria. JREEN 21:181–198
41. IRENA (2024) Renewable power generation costs in 2023. International Renewable Energy Agency, Abu Dhabi
42. Rodríguez-Gallegos CD, Gandhi O, Yang D et al (2018) A siting and sizing optimization approach for PV–battery–diesel hybrid systems. IEEE Trans Ind Appl 54:2637–2645. https://doi.org/10.1109/TIA.2017.2787680
43. Blank J, Deb K (2020) Pymoo: multi-objective optimization in python. IEEE Access 8:89497–89509. https://doi.org/10.1109/ACCESS.2020.2990567
44. Huang B, Cheng R, Li Z et al (2024) EvoX: a distributed GPU-accelerated framework for scalable evolutionary computation. IEEE Trans Evol Comput. https://doi.org/10.1109/TEVC.2024.3388550
45. Miller BL, Goldberg DE (1995) Genetic algorithms, tournament selection, and the effects of noise. Complex Syst 9:193–212
46. Blickle T, Thiele L (1996) A comparison of selection schemes used in evolutionary algorithms. Evol Comput 4(4):361–394. https://doi.org/10.1162/evco.1996.4.4.361
47. Deb K, Agrawal RB (1995) Simulated binary crossover for continuous search space. Complex Syst 9(2):115–148
48. Li W, Niliang Q, Wang L, Jiang Q (2024) Two-stage many-objective evolutionary algorithm: enhanced dominance relations and control mechanisms for separated balance. Complex Intell Syst 10:6509–6543. https://doi.org/10.1007/s40747-024-01505-0
49. Gelchu MA, Ehnberg J, Shiferaw D, Ahlgren EO (2023) Impact of demand-side management on the sizing of autonomous solar PV-based mini-grids. Energy 278:127884. https://doi.org/10.1016/j.energy.2023.127884
50. Bansal JC, Singh PK, Saraswat M et al (2011) Inertia weight strategies in particle swarm optimization. In: 2011 third world congress on nature and biologically inspired computing. IEEE, Salamanca, pp 633–640
51. Chang H, Sun Y, Lu S, Lin D (2024) A multistrategy differential evolution algorithm combined with Latin hypercube sampling applied to a brain–computer interface to improve the effect of node displacement. Sci Rep 14:20420. https://doi.org/10.1038/s41598-024-69222-9
52. Kukkonen S, Lampinen J (2005) GDE3: the third evolution step of generalized differential evolution. In: 2005 IEEE congress on evolutionary computation. IEEE, Edinburgh, pp 443–450

53. Storn R, Price K (1997) Differential evolution - a simple and efficient heuristic for global optimization over continuous spaces. J Glob Optim 11:341–359. https://doi.org/10.1023/A:1008202821328
54. Das S, Suganthan PN (2011) Differential evolution: a survey of the state-of-the-art. IEEE Trans Evol Comput 15:4–31. https://doi.org/10.1109/TEVC.2010.2059031
55. Zhang T, Li W, Wang R (2023) Surrogated-assisted multimodal multi-objective optimization for hybrid renewable energy system. Complex Intell Syst 9:4075–4087. https://doi.org/10.1007/s40747-022-00943-y
56. Long W, Dong H, Wang P et al (2023) A constrained multi-objective optimization algorithm using an efficient global diversity strategy. Complex Intell Syst 9:1455–1478. https://doi.org/10.1007/s40747-022-00851-1
57. Deb K, Pratap A, Agarwal S, Meyarivan T (2002) A fast and elitist multiobjective genetic algorithm: NSGA-II. IEEE Trans Evol Comput 6:182–197. https://doi.org/10.1109/4235.996017
58. Gu Q, Wang Q, Xiong NN et al (2022) Surrogate-assisted evolutionary algorithm for expensive constrained multi-objective discrete optimization problems. Complex Intell Syst 8:2699–2718. https://doi.org/10.1007/s40747-020-00249-x
59. Das I, Dennis JE (1998) Normal-boundary intersection: a new method for generating the Pareto surface in nonlinear multicriteria optimization problems. SIAM J Optim 8:631–657. https://doi.org/10.1137/S1052623496307510
60. Li K (2024) A survey of multi-objective evolutionary algorithm based on decomposition: past and future. IEEE Trans Evol Comput. https://doi.org/10.1109/TEVC.2024.3496507
61. Zhang Q, Li H (2007) MOEA/D: a multiobjective evolutionary algorithm based on decomposition. IEEE Trans Evol Comput 11:712–731. https://doi.org/10.1109/TEVC.2007.892759
62. He C, Huang S, Cheng R et al (2021) Evolutionary multiobjective optimization driven by generative adversarial networks (GANs). IEEE Trans Cybern 51:3129–3142. https://doi.org/10.1109/TCYB.2020.2985081
63. Li K, Deb K, Zhang Q, Kwong S (2015) An evolutionary many-objective optimization algorithm based on dominance and decomposition. IEEE Trans Evol Comput 19:694–716. https://doi.org/10.1109/TEVC.2014.2373386
64. Li W, Zhang G, Zhang T, Huang S (2020) Knee point-guided multiobjective optimization algorithm for microgrid dynamic energy management. Complexity 2020:8877008. https://doi.org/10.1155/2020/8877008
65. Yu G, Ma L, Jin Y et al (2022) A survey on knee-oriented multiobjective evolutionary optimization. IEEE Trans Evol Comput 26:1452–1472. https://doi.org/10.1109/TEVC.2022.3144880
66. Zhao L, Ren Y, Zeng Y et al (2022) A knee point-driven many-objective pigeon-inspired optimization algorithm. Complex Intell Syst 8:4277–4299. https://doi.org/10.1007/s40747-022-00706-9
67. Borges CLT, Pinto RJ (2008) Small hydro power plants energy availability modeling for generation reliability evaluation. IEEE Trans Power Syst 23:1125–1135. https://doi.org/10.1109/TPWRS.2008.926713
68. Thakur C, Teutschbein C, Kasiviswanathan K, Soundharajan B-S (2024) Mitigating El Niño impacts on hydro-energy vulnerability through identifying resilient run-of-river small hydropower sites. J Hydrol Reg Stud 51:101622. https://doi.org/10.1016/j.ejrh.2023.101622
69. Paschetto A, Caselle C, Bonetto SMR (2025) A GIS-based methodology for hydropower potential assessment: balancing energy production and ecosystem sustainability. Environ Chall 20:101236. https://doi.org/10.1016/j.envc.2025.101236
70. Bhattarai SB, Shrestha RM (2023) Analysis of implications of a regulation on design discharge of run-of-river hydropower projects in Nepal. Sustain Water Resour Manag 9:80. https://doi.org/10.1007/s40899-023-00860-z
71. Gasore G, Santos A, Ntagwirumugara E, Zimmerle D (2023) Sizing of small hydropower plants for highly variable flows in tropical run-of-river installations: a case study of the Sebeya River. Energies 16:1304. https://doi.org/10.3390/en16031304
72. SOLARGIS Solar irradiance data | Solargis. https://solargis.com/. Accessed 30 Aug 2023
73. Kavuma C, Sandoval D, de Dieu HKJ (2022) Analysis of solar photo-voltaic for grid integration viability in Uganda. Energy Sci Eng 10:694–706. https://doi.org/10.1002/ese3.1078
74. Sawle Y, Jain S, Babu S et al (2021) Prefeasibility economic and sensitivity assessment of hybrid renewable energy system. IEEE Access 9:28260–28271. https://doi.org/10.1109/ACCESS.2021.3058517
75. Electricity Regulatory Authority (ERA) (2023) Renewable energy feed-in-tariffs (REFIT VI). Electricity Regulatory Authority, Kampala
76. Electricity Regulatory Authority (2025) Notice of amendment of Uganda renewable energy feed-in tariff (REFiT) guidelines (Phase VI). The Uganda Gazette, Vol. CXVIII, No. 28, General Notice No. 950 of 2025, 4 April 2025, p. 1023. Kampala: Uganda Printing and Publishing Corporation. https://www.era.go.ug. Accessed 31 Aug 2025
77. Elsner C, Neumann M, Müller F, Claar S (2022) Room for money or manoeuvre? How green financialization and de-risking shape Zambia's renewable energy transition. Can J Dev Stud/Revue canadienne d'études du développement 43:276–295. https://doi.org/10.1080/02255189.2021.1973971
78. Eberhard A, Naude R (2016) The South African Renewable Energy Independent Power Producer Procurement Programme: a review and lessons learned. J Energy South Afr 27:1. https://doi.org/10.17159/2413-3051/2016/v27i4a1483
79. Mac Clay P, Börner J, Sellare J (2023) Institutional and macroeconomic stability mediate the effect of auctions on renewable energy capacity. Energy Policy 180:113685. https://doi.org/10.1016/j.enpol.2023.113685
80. Del Río P, Kiefer CP (2023) Academic research on renewable electricity auctions: taking stock and looking forward. Energy Policy 173:113305. https://doi.org/10.1016/j.enpol.2022.113305
81. Apfel D (2022) Renewable energy transition in Senegal? Exploring the dynamics of emerging paths to a sustainable energy system. Energy Res Soc Sci 92:102771. https://doi.org/10.1016/j.erss.2022.102771
82. International Finance Corporation (IFC) (2022) IFC and partners invest $1.1 Billion to build the largest solar plant and wind farm in Egypt. World Bank Group
83. Ghali M, Ibrahiem DM (2023) Quantifying the saved social costs of the solar energy projects funded by the EBRD in Egypt. IJEEP 13(5):365–373. https://doi.org/10.32479/ijeep.14807